Study for the timing mechanism of a spiking network model of the cerebellum

by
Takeru Honda

Submitted in Partial Fulfillment
of the requirements for the Degree of
DOCTOR OF ENGINEERING

at
The University of Electro-Communications

June 2011

Study for the timing mechanism of a spiking network model of the cerebellum

Approve by Supervisor Committee:

Chairperson: Professor Tetsuro Nishino

Member: Professor Haruhisa Takahashi

Member: Professor Satoshi Kobayashi

Member: Professor Yutaka Sakaguchi

Member: Associate Professor Hayaru Shono

概要

小脳は運動制御を担っている．特に，いつ運動を開始し終了するかについてのタイミングを小脳が制御していることが，瞬目反射の条件付けという実験課題でよく調べられている．瞬目反射の条件付けとは，音 (conditioned stimulus，CS) とまぶたへの侵害刺激 (unconditioned stimulus，US) の組み合わせを繰り返し与えると，音だけでまぶたを閉じる (conditioned response，CR) 条件反応の学習である．CS-US 間の時間間隔を変えて条件付けを行うと，まぶたを閉じるまでの時間がそれに応じて変化することから，小脳のどこかで時間の情報が表現されていると考えられる．1 つの可能性は顆粒細胞とゴルジ細胞を含む小脳の顆粒層であり，時間をコードできる小脳顆粒層モデルが多く提案されている．その一つとして，再帰的な抑制性のネットワークを形成している顆粒細胞ーゴルジ細胞間にランダム結合を仮定し，ゴルジ細胞に NMDA チャネルを仮定することによって，顆粒細胞集団の発火パターンで CS 呈示開始からの時間経過を表現できる Random Projection Model が提案されている．このモデルではランダム結合によって各顆粒細胞がランダムにバースト発射と停止を繰り返す．異なる顆粒細胞は異なるタイミングで間欠的にスパイク発射と停止を繰り返すため，ある時刻で発火する細胞は集団として一意に定まり，その集団は別の時刻では集団として現れない．つまり，一時刻と一細胞集団を一対一に対応づけることで，CS 呈示開始からの時間経過を表現できる．

一方，動物が静止状態にあるとき，小脳顆粒層の local field potential (LFP) はラットの場合 7-8Hz 程度，サルの場合 13-18Hz 程度で振動していることが報告されている．この振動の源は不明であるが，小脳顆粒層の再帰ネットワークによって顆粒細胞とゴルジ細胞が同期的かつ周期的に発火し，それによって LFP の振動が現れるとするモデルが提案されている．

小脳への入力は，苔状線維を介して顆粒細胞に与えられる．ラットの瞬目反射の条件付けにおいて，CS が呈示されている間は苔状線維は 30Hz 程度で発火し，CS が呈示されていない間，つまり動物が静止している間は 5Hz 程度で自発発火することが発見されている．よっ

て上記の二つのモデルから，苔状線維の発火頻度に応じて CS 呈示開始からの時間経過を表現する状態 (時間表現状態) と細胞が同期して発火する状態 (同期発火状態) の間を遷移することが期待されるが，前者のモデルでは時間経過を表現するのみであり，後者は同期発火しか示さなかった．

我々は様々な状況や環境で，時間の進み方を遅く感じたり早く感じたりすることがある．フェレットの瞬目反射の条件付けにおいて，条件付け後に CS の強度を強くすると，CR がより早く引き起こされることが報告されている．それは CS の強度に応じて CR までの時間の進み方が速くなっていることを示唆するが，そのメカニズムは明らかではない．そして，このメカニズムを説明できる小脳顆粒層モデルは未だ存在しない．

本研究では，顆粒細胞が同期発火状態を示すモデルと時間表現状態を示すモデルを統合した小脳顆粒層のスパイキングネットワークモデルを構築した．特に，ゴルジ細胞の樹状突起上に電位依存性のある NMDA チャネルを仮定した．入力刺激が弱いとき顆粒細胞は 9Hz の同期発火状態を示し，入力刺激が強いとき時間表現状態を示すことを示唆した．ゴルジ細胞の NMDA チャネルの電位依存性の効果を除くと，その 2 状態の遷移が見られなかった．このことは，小脳顆粒層で見られる LFP の振動と瞬目反射の条件付けに重要な時間経過の表現との切り替えにおいて，NMDA チャネルの電位依存性が重要な役割を担っていることを示唆する．

さらに，時間表現状態を示す範囲内で CS の強度を強くすると，顆粒細胞の活動集団が早く現れ，そして，異なる集団へとより早く遷移した．この結果は強い CS を与えると内部時計刻みが促進されることを示唆した．ゴルジ細胞の NMDA チャネルの電位依存性の効果を除くと，強い CS を与えても顆粒細胞の活動集団は早い遷移は見られなかった．よって，内部時計刻みの促進は NMDA チャ ネルの電位依存性によって引き起こされることが示唆された．我々は，さらに，瞬目反射の 条件付けのシミュレーションを行い，CR のタイミングの変化を調べた．CS が与えられると顆粒細胞は時間経過を表現し，プルキンエ細胞では US 入力のタイミングの前後でスパイク発射を停止し CR のタイミングを学習した．学習後，強い CS を与えると顆粒細胞の活動集団が異なる集団へとより早く遷移するため，CR のタイミングが早まった．以上より，CR のタイミングの変化は小脳顆粒層を含むネットワークによって実現されることが示唆された．

Abstract

We built a spiking network model of the cerebellar granular layer and analyzed its dynamics. Assuming N-methyl-D-aspartate (NMDA) channels on the dendrites of model Golgi cells, we found that the voltage-dependent synaptic transmission through the channels controlled the transition of activity states of model granule cells. That is, when input stimuli to granule cells were weak, the granule cells synchronously fired at around 9Hz (Synchronized oscillation state); when input stimuli were strong, they exhibited random alternations between burst and silent modes. The population of spiking granule cells changed gradually with time, and did not appear more than once. Because there was no recurrence in the generated sequence, the sequence of populations represented the passage of time (POT) (POT-representing state). Taken together, it is suggested that the dynamics of the cerebellar granular layer is controlled by the strength of mossy fiber input.

Furthermore, it was possible to speed up/slow down the sequence generation as the strength of input stimuli increases/decreases in POT-representing state. This is because a time constant of NMDA channels on Goc dendrites was changed with strength of input stimuli by the voltage-dependence of the NMDA channels. When the voltage-dependence was blocked, it was impossible to change the clock speed. Therefore, it is suggested that the speed of the sequence generated from the cerebellar granular layer is controlled by the strength of mossy fiber input.

Finally, we performed simulations of delay eyeblink conditioning in the representation of POT between onsets of conditioned and unconditioned stimuli. We added a model Purkinje cell and inhibitory cell (stellate cell or basket cell) to the present model and simulated long-term depression and potentiation at parallel fiber-Purkinje cell synapses and parallel fiber-inhibitory cell synapses. We observed that the PC successfully learned

to stop firing at the onset of the unconditioned stimulus and the timing of the stop changed by the strength of mossy fiber input. This suggests that the timing of the condition response is controlled by the strength of mossy fiber input in delay eyelid conditioning. Thus, this phenomenon may be generated by a network include the cerebellar granular layer.

Acknowledgements

First of all I would to thank my supervisor, Professor Testuro Nishino, for his guidance and support. His constructive inputs and invaluable advice have made it easy to track a field of research and helped to complete the dissertation. His insightful comments and suggestions have been invaluable. I also wish to thank him specially for the scientific freedom that he gave me to explore new paths.

I'm deeply indebted to Professor Shigeru Tanaka for his support, guidance and inspiration. His invaluable comments and suggestions helped to improve my ideas and modify our paper. I'm also grateful to Dr. Tadashi Yamazaki who belongs to RIKEN BSI Toyota-BSI collaboration for his help in writing some parts of codes for analyses and valuable comments. It was really great fun to work together and to be able to share discussions. I wish to express my warm and sincere thanks to Professor Soichi Nagao, Team leader of RIKEN BSI Motor learning control laboratory, who supported our study and give me valuable advices. I'm also thankful to all my colleagues in Nishino laboratory and Nagao laboratory (Motor learning control lab.) for their individual help.

I would like to thank all the members of the doctoral committee: Professor Testuro Nishino, Professor Haruhisa Takahashi, Associate Professor Hayaru Shono, Professor Satoshi Kobayshi, and Professor Yutaka Sakaguchi. Their suggestions and criticism had been essential for the preparation of this dissertation.

Contents

Chapter 1

Introduction

Human beings act, learn, feel and think using various parts of the brain which is the best computer in a human body. Although many researchers have conducted various experiments, nobody knows yet how human beings can generate or control these actions. The understanding of the brain mechanism for this question may lead to finding a theoretical model which has more computational power than the present computer based on a Turing machine, or developing new methods for artificial muscle actuators which are out of control in the present technology.

Some functions of even part of the brain have been known through many experiments. Specially, it is discovered that the cerebellum included in the brain controls movements of muscles. We think that algorithm and idea based on this cerebellar mechanism may apply to control system of the artificial muscle actuators. We focus on the cerebellum in the present study because the number of kinds of the cerebellar cells is smaller and the cerebellar structure is more simple than other parts of the brain. Although the cerebellum is well researched in experiments of molecular, anatomy, physiology and behavior, the present science has not clarified yet how the cerebellum can generate cerebellar functions. Our purpose is to propose a cerebellum model founded on the experimental data and to explain some cerebellar functions using computer simulations. Our findings in the process may help development of robot control system including artificial muscle actuators.

1.1 Organization of the present thesis

From next section, we introduce the cerebellum anatomy and the cerebellar function in order to easily understand our spiking network model which is denoted in chapter 2. In chapter 3 we show equations and mathematical functions using the present study in order to analyze firing patterns. We describe about stimulus-strength-dependent state transition (related with Honda et al., 2008) in chapter 4. Moreover, we summarize stimulus-strength-dependent timing control (related with Honda et al., 2010) in chapter 5. Finally, we discuss about results of our study.

1.2 Cerebellum

Compared with neurons in other parts of brain, physiological property and circuit of most cerebellar neurons is well known. In this chapter, we first summary cerebellar anatomical division, circuit, and input to the cerebellar cortex. Furthermore, we describe the cerebellar learning which Ito (1984) found. Finally, we introduce two cerebellar functions in animal behaviors.

The cerebellum (in Latin, it means little brain) which is located at dorsal part of the brain stem, constitutes only 10% to 15% of the total weight of the whole brain (14.2% in rats and 10.5% in humans) (Ito, 1984) but contains more than half of all its neurons.

These neurons are arranged in a highly regular manner as repeating units, each of which is a basic circuit module, called cerebellar corticonuclear microcomplexes. A microcomplex consists of four components: (1) a microzone of the cerebellar cortex as denned by the late Oscarsson (1976), (2) a small group of neurons in vestibular or cerebellar nuclei receiving Purkinje cell inhibition from the microzone, (3) bundles of cerebellar afferent fibers arising from smoll groups of precerebellar structures and supplying excitatory synapses to the nuclear neurons and mossy fiber terimals to the microzone and (4) a bundle of fibers originating from a small group of inferior olive neurons and supplying climbing fibers to the microzone and excitatory synapses to the nuclear neurons. Despite its structural regularity the cerebellum is divided into several distinct regions, each of which receives projections from different portions of the brain and spinal cord and projects to different

motor systems. These features suggest that regions of the cerebellum perform similar computational operations but on different input.

The cerebellum is characterized with respect to three viewpoints which are input, output and plasticity. First, the cerebellum is provided with extensive information about the goals, commands, and feedback signals associated with the programming and execution of movement. This input is important because the number of projections into the cerebellum is 40 times more than that of output projections from the cerebellum. Second, the output projections of the cerebellum are focused mainly on the premotor and motor systems of the cerebral cortex and brain stem, systems that control spinal interneurons and motor neurons directly. Third, synaptic transmission in the circuit modules can be modified, a feature that is crucial for motor adaptation and learning. Based on three aspect of this cerebellar organization, the cerebellum influences the motor systems by evaluating disparities between intention and action and by adjusting the operation of motor centers in the cortex and brain stem while a movement is in progress as well as during repetitions of the same movement.

Removal of the cerebellum does not alter sensory thresholds or the strength of muscle contraction. Thus the cerebellum is not necessary to basic elements of perception or movement. Rather, damage to the cerebellum disrupts the spatial accuracy and temporal coordination of movement. It markedly impairs not only balance and reduces muscle of movement but also motor learning and certain cognitive functions. Therefore, the cerebellum plays a central role in motor control which consists of timing and gain control. Timing control decides when the movement should star or stop. Gain control coordinates how range muscles should move. We propose Eq(1.1) as follows:

$$\text{Motor control} = \text{Timing control} \times \text{Gain control}. \tag{1.1}$$

1.3 Cerebellar Anatomy

Cerebellar cortex and nuclei

The cerebellum which occupies most of the posterior cranial fossa is composed of an outer mantle of gray matter (the cerebellar cortex), internal white matter, and the three pairs of deep nuclei: the **fastigial**, the **interposed** (itself composed of two nuclei, the **globose** and **emboliform**), and the **dentate**. It is connected to the dorsal aspect of the brain stem by three symmetrical pairs of tracts: the **inferior cerebellar peduncle** (also called the restiform body), the **middle cerebellar peduncle** (or brachium pontis), and the **superior cerebellar peduncle** (or brachium conjunctivum) (Figure 1.1). The superior cerebellar peduncle contains efferent fibers from the dentate, emboliform, and globose nuclei. These are the axons that send feedback to the motor cortex in the frontal lobe via the red nucleus in the midbrain and the thalamus. Afferent fibers traveling in this peduncle take proprioceptive information to the cerebellum from the lower body. This information ascends along the spinal cord in the ventrospinocerebellar tract, before entering the cerebellum. The middle cerebellar peduncle is the largest of the peduncles and links the cerebellum with the pons. Via this connection, the cerebellum receives a copy of the information for muscle movement that the pyramidal tract is carrying down to lower motor neurons. The inferior cerebellar peduncle connects the cerebellum with the medulla, but also to the **vestibular nuclei** located in the lower pons and medulla and with cells of the reticular formation. Proprioceptive information from the upper body, traveling along the dorsospinocerebellar tract enters the cerebellum on the inferior cerebellar peduncle.

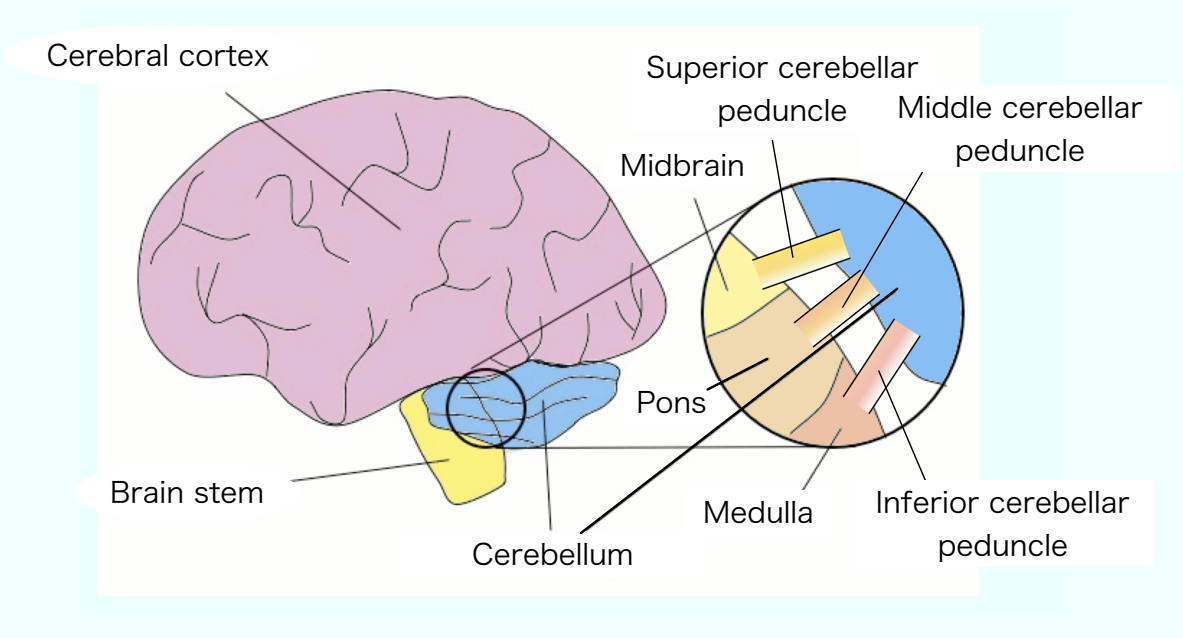

Figure 1.1: The pathway between the cerebellum and brain stem. The cerebellum is connected to the brain stem by the inferior cerebellar peduncle, the middle cerebellar peduncle, and the superior cerebellar peduncle.

1.3.1 Cerebellar anatomical division

A Striking feature of the surface of the cerebellum is the presence of many parallel convolutions called **cerebellar folia** (Latin, leaves) that run from side to side and divided by many **cerebellar fissures** (Table 1.1). Two deep transverse fissures divide the cerebellum into three lobes. The **primary fissure** on the dorsal surface separates the **anterior lobe** and **posterior lobe**, which together form the body of the cerebellum. The **posterolateral fissure** on the ventral surface separates the body from the much smaller **flocculonodular lobe**. Moreover, the cerebellar fissures separated the cerebellum from ten cerebellar folium (Lobule I – Lobule X) (Table 1.1). Sagittal section through the midline shows that shallower fissures further subdivide each lobe into several lobules comprising a variable number of folia.

Two longitudinal furrows, which are most prominent ventrally, distinguish three mediolateral regions that are important functionally. The furrows define an elevated ridge in the midline known as the **vermis** (Latin, worm) (median vermal area) which projects into the fastigial nuclei. On either side of the vermis are the **cerebellar hemispheres**, each of which is divided into intermediate (paravermal area) and lateral regions. The intermediate, lateral area and flocculonodular lobe project into the interposed, dentate and vestibular nuclei, respectively. The three mediolateral regions of the body of the cerebellum (the vermis and intermediate and lateral parts of the hemispheres) and the **flocculonodular lobe** divided by nuclei into which to cerebellar cortex output receive different afferent inputs, project to different parts of the motor systems, and represent distinct functional subdivisions.

The flocculonodular lobe is the most primitive part of the cerebellum, appearing first in fishes. Its cortex receives input directly from primary vestibular afferents and projects to the lateral vestibular nuclei. In higher vertebrates its function is limited to controlling balance and eye movements and thus called the **vestibulocerebellum**.

The vermis and hemispheres develop later in phylogeny. The vermis receives visual, auditory, and vestibular input as well as somatic sensory input from the head and proximal parts of the body. It projects by way oth the fastigial nucleus to cortical and brain stem regions that gives rise to the medial descending systems that control proximal muscles of the

Table 1.1: The cerebellar anatomical division and cerebellar fissures

Lobule number	virmis	cerebellar hemisopheres
Lobule I	lingula cerebelli	nothing
Lobule II, III	central lobule	ala of central lobule
Lobule IV, V	culmen	quadrangular lobule
Primary fissure		
Lobule VI	declive	simple lobule
Lobule VII	folium vermis	superior semilunar lobule
Horizontal fissure		
Lobule VII	tuber vermis	inferior semilunar lobule
Lobule VIII	pyramis vermis	biventer lobule
Secondary fissure		
Lobule IX	uvula vermis	cerebellar tonsil
Posterolateral fissure		
Lobule X	nodulus	flocculus

body and limbs. The vermis governs posture and locomotion as well as gaze. The adjacent intermediate partof the hemisphere also receives somatosensory input from the limbs. This region projects via the interposed nucleus to lateral corticospinal and rubrospinal systems and thus controls the more distal muscles of the limbs and digits. Because the vermis and intermediate hemispheres are the only regions to receive somatosensory inputs from the spinal cord, they are often called the the **spinocerebellum**.

The lateral parts of the hemispheres, which are phylogenetically most recent, are much larger in humans and apes than in monkeys or cats. This region receives input exclusively from the cerebral cortex through the pontine nuclei and is thus called the **cerebrocerebellum** (**pontocerebellum**). Its output is mediated by the dentate nucleus, which project to motor, premotor, and prefrontal cortices. Recent imaging data indicate that the cerebrocerebellum is intimately involved in in planning and mental rehearsal of complex motor actions and in the conscious assessment of movement errors.

1.3.2 Cerebellar circuit

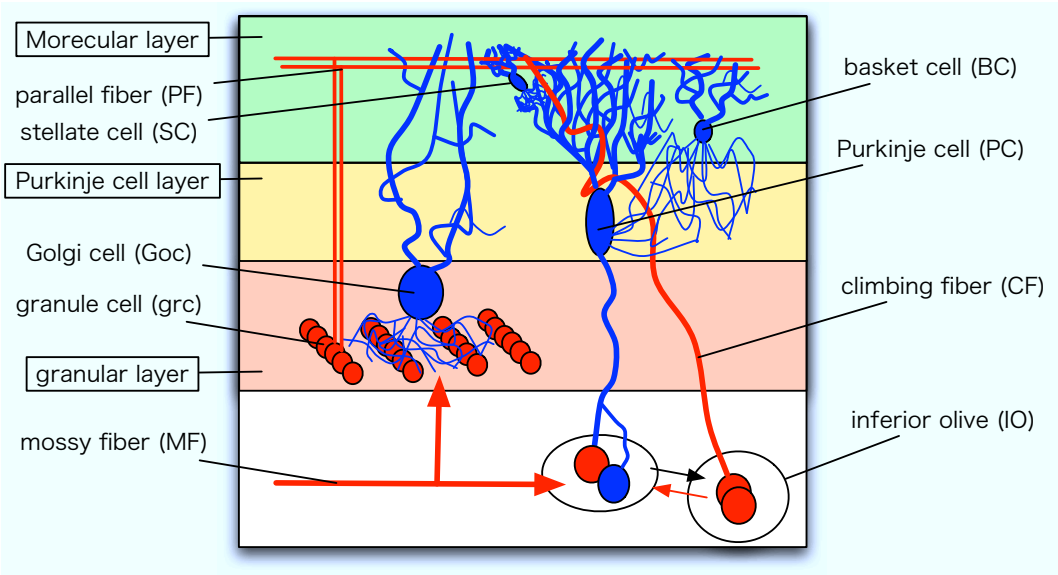

Figure 1.2: The cerebellar circuit. The cerebellar cortex is organized into three layers and contains five types of neurons.

The cerebellar cortex is a simple three-layered structure consisting of only several types of neurons: the inhibitory **Purkinje cell** (PC), **Golgi cell** (Goc), **stellate cell** (SC), and **basket cell** (BC); and the excitatory **granule cell** (grc) (Figure 1.2).

Molecular layer

The outermost or **molecular layer** of the cerebellar cortex contains the cell bodies of two types of inhibitory interneurons, the SCs and BCs, dispersed among the excitatory axons of grcs and the dendrites of inhibitory PCs whose cell bodyies lie in deeper layers (Figure 1.2). Especially, SC somas are located in the external two-thirds of the molecular layer while BC somas are in the internal third. These interneurons receive excitatory inputs from grcs as well as from **climbing fibers** (CFs). Inhibitory axons of SCs tent to run parallel to the Purkinje cell Layer (Palay and Chan-Palay, 1974). A SC inhibits not only PC dendrites but also around 4 other SCs within a distance of 100 μm from the soma whose diameter is about 8 μm in rats (Kondo and Marty, 1998). The axons of the grcs in this layer run parallel to the long axis of the folia and therefore are called **parallel fiber**s (PF) whose length is around 5 mm in a turtle (Mugnaini, 1983; Pichitpornchai et al., 1994). The dendrites of the PC are oriented perpendicular to these axons. SCs and BCs are facilitated by PFs.

Purkinje cell layer

Beneath the molecular layer is the **Purkinje cell layer**, consisting of a single layer of PC bodies. PCs have large cell bodies (50–80 μm) and fan-like dendritic arborizations that extend upward into the molecular layer. Their axons project into the underlying white matter to the deep cerebellar or vestibular nuclei and provide the output of the cerebellar cortex. This output is entirely inhibitory and mediated by the neurotransmitter γ-aminobutyric acid (GABA) The short axons of SCs contact the nearby dendrites of PCs and the long axons of BC run perpendicular to the PFs and form synapses with PC anterior and posterior to the PF beam. This arrangement–facilitation of a central array of neurons and inhibition of surrounding cells by local input–resembles the center-surround antagonism in visual and somatosensory pathways.

Granular layer

The innermost or **granular layer** contains a vast number (estimated at around 6,224,000 grcs per 1 cu.mm of granular substance in a cat (Palkovits et al., 1971)) of grcs (so called because they appear as small and densely packed darkly stained nuclei in histological section) and a few larger Gocs (estimated at around 980 Gocs per 1 cu.mm of granular substance in a cat (Palkovits et al., 1971). The average thickness of the granular layer is around 255 μm in a cat (Palkovits et al., 1971). The mossy fibers, the major source of afferent input to the cerebelum (see below), terminate in this layer. The bulbous terminals of the mossy fibers contact grcs and Gocs in synaptic complexes calle **cerebellar glomeruli**.

The Goc has an elaborate dendritic tree in the overlying molecular layer. The GABA-ergic terminals of Gocs form axodendritic synapses with the grcs in the glomeruli. Goc firing, initiated by firing in the PFs, suppresses mossy fiber excitation of the grcs and thus tends to shorten the duration of bursts in the PFs.

1.3.3 Input to the cerebellum from fibers

The cerebellum receives two main types of afferent inputs, **mossy fiber**s (MFs) and **climbing fiber**s. Both groups of fibers form excitatory synapses with cerebellar neurons, but the two groups terminate differently in the cerebellar cortex and produce different patterns of firing in the PCs. MFs and CFs respond very differently to sensory stimulation and during motor activity.

Mossy fibers

MFs originate from nuclei in the spinal cord and brain stem and carry sensory information from the periphery as well as information from the cerebral cortex. They terminate as excitatory synapses on the dendrites of grcs in the granular layer (Figure 1.2). The axons of the grcs (PFs) travel long distances (up to one-third of the width of the cerebellar hemisphere) along the long axis of the cerebellar folia in the molecular layer, thus exciting large numbers of PCs in the same transverse plane (Figure 1.2). In humans each PC receives input from as many as one million granule cells, each of which collects input from many MFs. Spontaneous activity in MFs produces steady stream of simple spike

in PCs. Somatosensory, vestibular, or other sensory stimuli change the frequency of the simple spike, which may reach several hundred spikes per second. Voluntary eye or limb movements are also associated with a marked change in frequency. Thus the frequency of simple spikes can readily encode the magnitude and duration of peripheral stimuli or centrally generated behaviors.

Climbing fibers

CFs originate from the inferior olivary nucleus and convey somatosensory, visual, or cerebral cortical information. The climbing fibers are so named because the wrap around the cell bodies and proximal dendrites of PCs like a vine on a tree, making numerous synaptic contacts. Individual PCs receive synaptic input from only a single SF, whereas each CF contacts 1–10 PCs. The terminals of the CFs in the cerebellar cortex are arranged topographically; the axons of clusters of olivary neurons terminate in thin parasagittal strips that extend across several folia. In turn, the PC within each strip project to common groups of deep nuclear neurons. This highly specific connectivity of the CF system contrasts markedly with the massive convergence and divergence of the MFs and PFs.

The basic circuit of the cerebellum is illustrated in Figure 1.2, which shows the excitatory and inhibitory connections between different cell types. The geometry of the principal connection–the MF, PF, and CF system–is shown in Figure 1.2.

CFs have unusually powerful synaptic effects on PCs. Each action potential in a climbing fiber generates a prolonged voltage-gated calcium conductance in the soma and dendrites of the postsynaptic PC. This results in prolonged depolarization that produces a **complex spike**: an initial large-amplitude spike followed by a high-frequency burst of smaller-amplitude action potentials. In contrast, PFs produce a brief excitatory postsynaptic potential that generates a single action potential or **simple spike**. Consequently, spatial and temporal summation of inputs from several PFs are needed before the PC will fire.

Climbing fibers fire spontaneously at very low rates, and these spontaneous rates are changed only modestly by sensory stimuli or during active movement. The frequency of complex spikes in PCs is rarely more than 1–3 per second. Such low frequencies cannot

by themselves carry substantial information about the magnitude of natural stimuli or behavior.

What could be encoded by the complex spikes? One possibility is that complex spikes might signal the timing of peripheral events or act as triggers for behavior. Linás (1985) has suggested that a form of timing signal might be provided by the synchronous firing of multiple PCs. Neurons in the inferior olivary nucleus are often electrotonically connected to one another through dedrodendritic synapses and therefore can fire in synchrony. The synchronous inputs of olivary neurons in CFs produces complex spikes in many PCs at almost the same time.

Interestingly, the electrotonic coupling of olivary neurons is under efferent control by GABA-ergic fibers from the cerebellar nuclei terminating in the olivary nucleus (Figure 1.2). By functionally, disconnecting certain olivary neurons through inhibition the nervous system could be selecting a specific array of PCs for synchronous activation. This idea is supported by cell recordings in which different patterns of synchronous discharge in different sets of PCs are correlated with different phases of a natural behavior. Thus, althoug there is little divergence of CFs, synchronization of inputs may allow populations of postsynaptic neurons with different inputs to act cooperatively.

1.3.4 Plasticity in the Cerebellar cortex

Despite the low frequency of their dicharge, climbing fibers may alter cerebellar output by modulating the synaptic effect of PF input to PCs in to ways. First, CF action potentials slightly reduce the strength of the PF inout to the PC. Thus, experimental lesions or localized cooling of the inferior olivary nucleus produce a large increase in the frequency of simple spikes generated in the PCs by the PFs.

Second, activity in CFs can induce selective **long-term depression** (**LTD**) in the synaptic strength of PF that are active concurrently. LTD has been analyzed in slices of cerebellum in which PC responses to concurrent stimulation of CFs and PFs can be recorded intracellularly. Ito (1984) found that concurrent stimulation of CFs and one set of PFs depresses the effect of later stimulation of the same PFs but has no effect on the stimulation of another set of PFs. For this depression to occur, however, the PF's simple

spike must occur within some 100–200 ms of the CF's complex spike.

The resulting depression can last minutes to hours and depends critically on the prolonged depolarization and large influx of calcium produced by the CF in PC dendrites. This long-term effect of the CF on the transmission of signals from the MF, grc, and PF through to the PC may be important in the cerebellar role in motor learning.

1.4 Behavior related with the cerebellum

1.4.1 LFP Oscillation in Cerebellar Granular Layer

Local field potential (LFP) oscillations at 10–40 Hz are present in preparation for movement in monkey parietal and motor cortices (Baker et al., 1997; Donoghue et al., 1998; MacKay and Mendonca, 1995; Murthy and Fetz, 1996; Rougeul et al., 1979). High-density recordings show that these LFPs represent the collective behavior of neurons surrounding the electrode (Csicsvari et al., 2003), and LFPs can carry a significant amount of information related to motor execution (Mehring et al., 2003; Pesaran et al., 2002). LFP oscillations at 10–25 Hz were also seen in the paramedian lobule of the cerebellum of the awake monkey (Courtemanche et al., 2002; Pellerin and Lamarre, 1997) and at 7–8 Hz (Hartmann and Bower, 1998; O'Connor et al., 2002), but also 15–16 Hz (O'Connor et al., 2002) in Crus II of the awake rat. These cerebellar oscillations are specific to the granular layer, when the animal is immobile, and are often stopped by movement (Pellerin and Lamarre, 1997; Hartmann and Bower, 1998). In the primate cerebellum, the paramedian lobule 10–25 Hz LFP oscillations are most prominent when the monkey is attentive and immobile, are closely related to multiunit grc firing and also PC simple spikes, are modulated during both left- and right-hand lever presses, but are also affected when the monkey is expecting reward without need of movement; these oscillations are thus state-related and differentially modulated during active or passive expectancy (Courtemanche et al., 2002).

1.4.2 Delay Eyeblink Conditioning

In Pavlovian delay eyeblink conditioning (for a review, e.g., (Mauk and Donegan, 1997; Hesslow and Yeo, 2002; Christian and Thompson, 2003)), an animal (e.g. rabbit, mouse,

and ferret) is exposed to the paired presentation of a sustained tone (conditioned stimulus: CS) and an airpuff (unconditioned stimulus: US) that induces the eyeblink reflex (Figure 2.1). After the repeated conditioning of CS-US presentation with a fixed interstimulus interval (ISI) between the onsets of the CS and US, the CS presentation alone causes the subject to close the eye as a conditioned response (CR) slightly prior to the US onset timing. This phenomenon indicates that the subject memorizes the ISI. When the subject's cerebellum is removed after the conditioning, the subject can not response at appropriate timing without the US. Electrolytic or ablation techniques have been used to establish the involvement of lobule HVI in conditioning. McCormick and Thompson (1984) first observed that lesions of much of the ipsilateral hemisphere of the cerebellar cortex (including HVI) did not abolish the response if the deep cerebellar nuclei were spared. They reported, however, that the cortical lesions affected the timing of the CR in some animals.

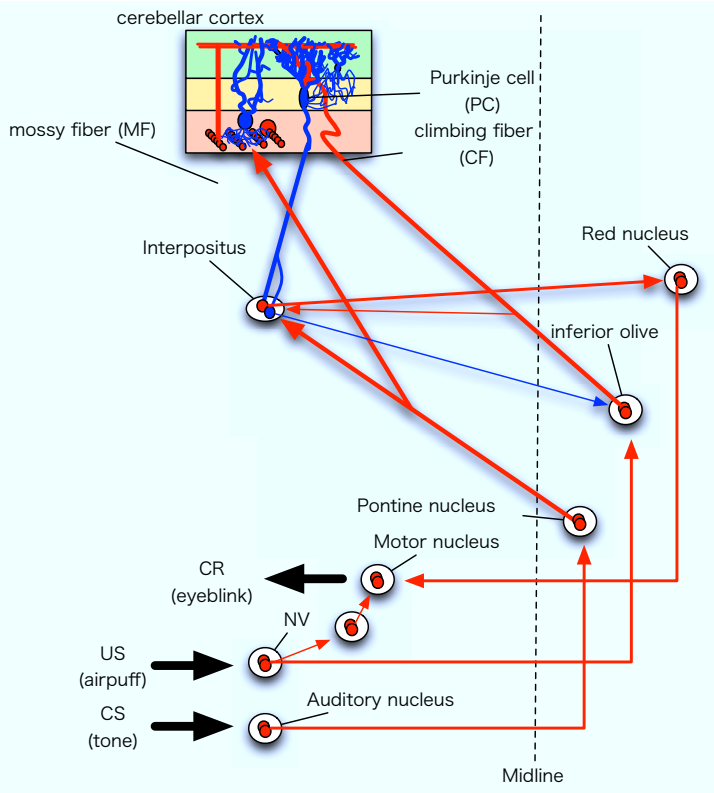

Figure 1.3: Simplified schematic (most interneurons omitted) of the putative essential circuitry for delay classical conditioning of eyeblink (and other discrete responses) learned with an aversive US (the sensory and motor nuclei activated depend of course on the nature of the CS and US—the more central portions of the circuit appear to be general). The reflex US–UR pathway involves direct and indirect projections from the trigeminal nucleus to the motor nuclei (for the eyeblink UR and CR primarily accessories 6 and 7). The tone CS pathway projects from auditory nuclei to the pontine nuclei and to the cerebellum as mossy fibers. The US pathway includes projections from the trigeminal to the inferior olive and to the cerebellum as climbing fibers. The CR pathway projects from the interpositus to the red nucleus and on to premotor and motor nuclei. There is also a direct GABAergic inhibitory projection from the interpositus to the inferior olive. Solid cell bodies and bar terminals indicate inhibitory neurons, open cell bodies and fork terminals indicate excitatory neurons. Stars indicate sites of plasticity based on current evidence. See text for details. (Modified from Thompson, 1986.)

Hesslow and colleagues (Hesslow and Ivarsson, 1994; Jirenhed et al., 2007) have recorded PC activity from the C3 zone ipsilateral hemispheral lobule VI during classical conditioning in decerebrate ferrets. They observed the gradual acquisition of inhibitory responses in PC simple spike firing as paired conditioning trials were given. Further, the inhibition occurred in later portions of the CS period as would be predicted if PCs are involved in conditioning. They also observed that PC response latencies changed as ISIs were altered and that the inhibition eventually decreased with extinction training. Mauk and colleagues (Kalmbach et al., 2010) have used micro-infusions during delay eyeblink conditioning in rabbits. Their results provide evidence that the expression of well-timed conditioned responses requires a well-timed decrease in the activity of PCs in anterior lobe.

The cerebellum and its associated circuitry constitute the entire essential circuit for delay classical conditioning of eyeblink and other discrete responses. A schematic depicting the entire essential circuitry for eye-blink conditioning is shown in Figure 1.3 (Thompson, 1986).

Several models of cerebellar plasticity have been proposed that are based on excitability changes at the PF–PC synapse as a result of co-activation of MFs and CFs, the two sensory input systems that project information into the cerebellum (e.g. Marr, 1969; Albus, 1971). In general, these models propose that when these fiber systems are co-activated, a long-term inhibition of PCs occurs that in turn causes a disinhibition of deep nuclear neuronal activity (because all PCs inhibit deep nuclear cells). The long-term decrease in PC excitability due to the conjunctive activation of MFs and CFs is called “long-term depression” (LTD) (Ito and Kano, 1982). Several studies have demonstrated an LTD effect at the PF–PCs synapses with conjunctive stimulation (Ekerot and Kanoa, 1985; Ito, 1984, 1989; Linden and Connor, 1991). Because MF (CS) and CF (US) co-activation appeared to be involved in classical eyeblink conditioning, these models of cerebellar plasticity seem to be applicable to this type of learning. Long-lasting excitatory plasticity has also been demonstrated in cerebellar cortex (e.g. Hirano, 1990; Jörntell and Ekerot, 2002) and possible potentiation processes at cerebellar synapses have been considered in models of cerebellar function (e.g. Attwell et al., 2001; Medina and Mauk, 2000). However, Nobody knows even if plasticity in cerebellar cortex is necessary for eyeblink classical conditioning and what role the cerebellar

cortex play in conditioning.

Chapter 2

Cerebellar Granular Layer Model

2.1 Network structure

We build a model granular layer of the cerebellum using the network structure employed in our previous study (Yamazaki and Tanaka, 2007a). That is, 32 × 32 model Gocs are arranged in two-dimensional grids (Figure 2.1A), which is in contrast with the one-dimensional arrangements of model Gocs and grcs in the study of Maex and De Schutter (Maex and De Schutter, 1998). Our model Gocs are evenly positioned at 35 μm intervals within a square sheet of 1,085 × 1,085 μm^2. It was estimated that there are 1,000 times more grcs than Gocs (Palkovits et al., 1971; Lange, 1974). Numerous grcs are connected with a glomerulus (Mugnaini et al., 1974). However, simulation with more than 1 million model neurons is beyond the power of our computers. In Yamazaki and Tanaka (2007a), 100 nearby grcs that were assumed to be connected with a glomerulus exhibited similar firing patterns despite the fact that each of the grcs independently received noisy signals through MFs. Such redundant activity patterns of grcs suggest that a large number of grcs behave as a single cluster when they receive inputs from the nearest Goc through a single glomerulus. In the present model, for the sake of the economy of computer power, we assume that a single model grc represents a grc cluster composed of about 1,000 neurons (Figure 2.1A).

We also assume that a model Goc randomly receives 10% of 9 × 32 PF inputs from model grcs with its dendritic arborization, whose diameter is set at 315 μm the Goc. The

mean and standard deviation of the actual number of PF inputs to a model Goc were 26.80 and 6.50, respectively(Figure 2.2A). Note that model Gocs do not receive MF inputs for simplicity. The model Goc, in turn, sends inhibitory inputs to model grcs located within the extent of axonal arborization (Figure 2.1B), which is set at 315 μm. The number of model Gocs located inside a circle of the diameter of 315 μm amounts to 69 by actual counting, which can be roughly estimated by $\pi(315/2)^2/(35-1)^2+1 = 68.4$. In the present model we assume that each grc randomly receives 10% of 69 connections from Gocs. The mean and standard deviation of the actual number of connections were 6.11 and 2.57, respectively (Figure 2.2B).

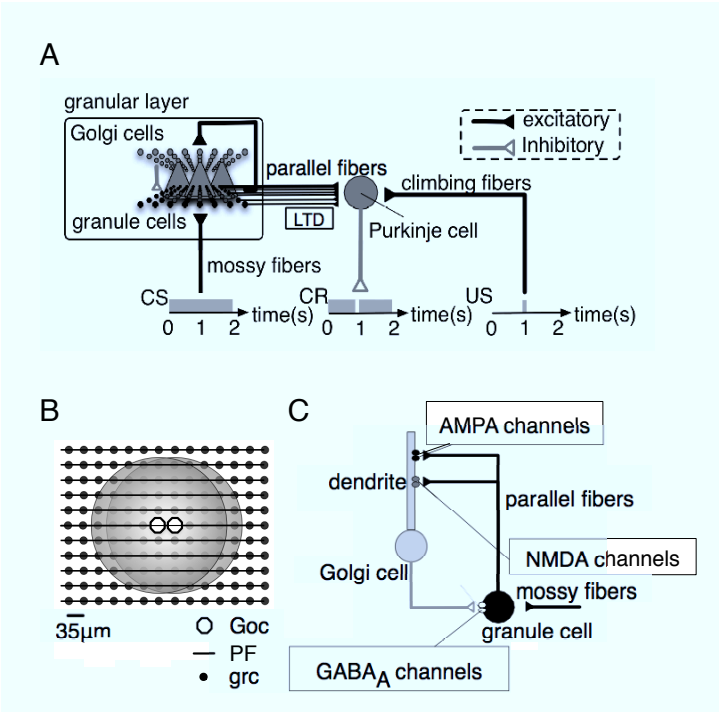

Figure 2.1: Schematic diagrams of the present cerebellar model and external input stimuli in delay eyeblink conditioning. A, During delay eyeblink conditioning, an animal receives the repeated paired presentation of a sustained tonal conditioned stimulus (CS) and an air-puff that is a delayed unconditioned stimulus (US) inducing an eyeblink response. Mossy fibers (MFs) convey CS signals to granule cells (grcs), which send excitation signals to Purkinje cells through parallel fibers (PFs), whereas climbing fibers (CFs) convey US signals to Purkinje cells (PCs). The Synaptic weights between PFs and Purkinje cells undergo long-term depression (LTD) when the PFs excite Purkinje cells at the timing of the signal input through CFs. After conditioning, the animal elicits an eyeblink as a conditioned response (CR) in response to a CS around the timing of the airpuff. B, 2-dimensional arrangement of grcs, Gocs and PFs in the model granular layer. Small dots and open circles indicate grcs and Gocs, respectively. Horizontal lines indicate PFs, which terminate at Goc dendrites, which are shown by gray disks. C, Synaptic channels that evoke potentials at grcs and Gocs. AMPA and NMDA channels are assumed to exist on the Goc dendrites, and $GABA_A$ channels are assumed to exist at grcs. A CS signal is simply modeled as a depolarizing current injection.

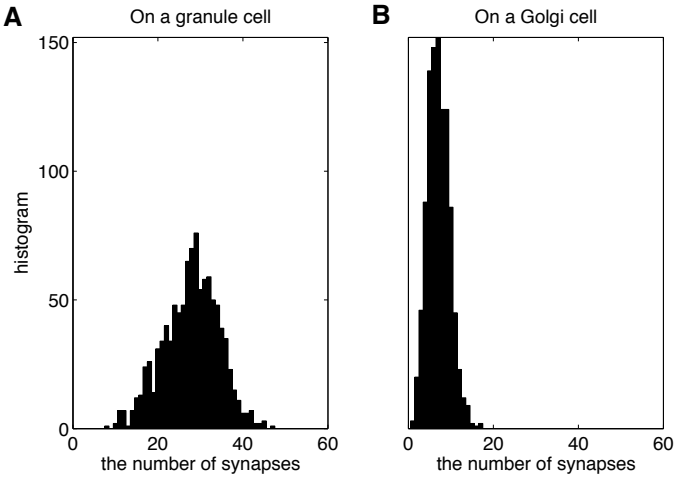

Figure 2.2: The number of Gocs (grcs) against the number of synaptic connections fed by grcs (Gocs) (A and B, respectively). On average, a Goc and a grc receive 26.80 (6.5) and 6.11 (2.57) inputs from grcs and Gocs, respectively (the numbers in the parents denote the standard deviation).

2.2 Model granule cells

We use the same model grcs as those adopted by Maex and De Schutter (1998) except for the synaptic channels. Brickley et al. (1999) reported that inhibitory postsynaptic potentials (IPSPs) can be fitted well with the sum of three exponentials, and that the largest component, which has the decay time constant of 100 ms, contributes to 20% of the IPSPs. Considering this finding, we simulate IPSPs using a double-exponential function with rise and decay time constants of 5 and 100 ms, respectively (Brickley et al., 1999). Further details are shown in Appendix.

2.3 Model Golgi cells

Maex and De Schutter (1998), a model Goc was also a single-compartment Hodgkin-Huxley unit with realistic ion channels. Their model Gocs received excitatory inputs from model grcs through α-amino-3-hydroxy-5-methyl-4-isoxazolepropionic acid (AMPA) channels with rise and decay time constants of 0.03 and 0.5 ms, respectively (Silver et al.,

1992).

It has been found that Gocs receive excitatory input signals from PFs through not only AMPA channels but also NMDA channels (Dieudonné, 1998). However, even when we add NMDA channels at the somas of model Gocs, the NMDA channels do not open effectively to evoke sustained depolarization because the after-hyperpolarization (AHP) (Wong and Stewart, 1992; Stuart and Sakmann, 1994) following the generation of each action potential rapidly decreases the somatic membrane potential. On the other hand, it is known that the dendritic potential tends not to be affected by AHP at cell somas (Wong and Stewart, 1992). Moreover, it has been shown that direct dendritic excitation produces sustained and burst responses although somatic excitation does not (Wong and Stewart, 1992). If NMDA channels really induce a prolonged activation of Gocs, it implies that NMDA channels are located on the Goc dendrites. In this study, a model Goc is represented as a soma and a dendrite whose length is 300 μm (cf. Ito, 1984) (Figure 2.1C). The dendrites of model Gocs are assumed to possess AMPA and NMDA channels. We simulate NMDA receptor (NMDAR)-mediated EPSPs with a double-exponential function with rise and decay time constants of 5 and 100 ms, respectively, in accordance with Misra et al. (2000). Further details are shown in Appendix.

It is known that Gocs are morphologically heterogeneous and their action potentials are variable (Geurts et al., 2003). However, we assume identical Gocs in the present model, because random connectivity in the network would have smeared individual heterogeneities.

2.4 Simulation tools

We build the present model and perform numerical simulations using the GENESIS simulator (Bower and Beeman, 1995). Differential equations are solved using the Crank-Nicolson method with a fixed time step of 20 μs. When we carry out simulation of eyeblink conditioning, we do not need to calculate activities of the granular layer at the same time. We have only to use activity patterns of grcs, which have been stored in a file recorded during the simulation of activities of the granular layer using GENESIS. Because we assume a simple PC model, the simulation does not require the usage of GENESIS that is an expert for simulation of realistic neuron models. Therefore, the simulation program of

the model PC for eyeblink conditioning, which is just solving differential equations using the first order Euler method with a fixed time step of 20 μs, was written in C and Ruby programming languages.

Chapter 3

Analyses of simulated results

3.1 Oscillation Index

Let $f_i(t)$ be the spike activity of model neuron (grc or Goc) $i(1 \leq i \leq N, N = 32 \times 32 = 1024)$ at time t:

$$f_i(t) = \begin{cases} 1 & \text{neuron } i \text{ elicits a spike at time } t, \\ 0 & \text{otherwise.} \end{cases} \tag{3.1}$$

The fluctuation in the number of neurons that elicit spikes at time t, $\delta f(t)$, is given by

$$\delta f(t) = \sum_{i=1}^{N} \Big[f_i(t) - \frac{1}{T} \sum_{t=-T/2}^{T/2} f_i(t) \Big], \tag{3.2}$$

The normalized autocorrelation function of the numbers of active neurons at times t and $t + \tau$ is defined by

$$NAC(\tau) = \frac{\sum_{t=-T/2}^{T/2} \delta f(t) \delta f(t+\tau)}{\sqrt{\sum_{t=-T/2}^{T/2} \Big[\delta f(t)\Big]^2} \sqrt{\sum_{t=-T/2}^{T/2} \Big[\delta f(t+\tau)\Big]^2}}, \tag{3.3}$$

where τ is a time lag and T is the duration of the spontaneous MF activity or the CS signal.

Calculating the normalized Fourier cosine transform of this normalized autocorrelation function, we define the oscillation index OI, which measures the degree of synchronized oscillation at neurons as follows:

$$OI = \frac{\sum_{t=-T/2}^{T/2} \cos(\xi t) NAC(t)}{\sum_{t=-T/2}^{T/2} NAC(t)}, \tag{3.4}$$

where ξ is the frequency giving a maximum power defined by the Fourier cosine transform of the normalized autocorrelation function. When OI takes a value of 1, a population of active neurons appears periodically. When OI takes a value of 0, $NAC(\tau)$ is a constant function of τ, and populations of active neurons appear uniformly in time.

3.2 Passage-of-time Index

$z_i(t)$ is defined as the AMPA receptor (APMAR)-mediated EPSPs on a Purkinje cell (PC) from grc i, as follows:

$$z_i(t) = \frac{1}{\tau_{\mathrm{PC}}} \sum_{s=0}^{t} \exp\left(-\frac{t-s}{\tau_{\mathrm{PC}}}\right) f_i(s), \tag{3.5}$$

where τ_{PC} is the decay time constant of AMPAR-mediated EPSPs at PCs, which is set at 30 ms. As defined in the previous study (Yamazaki and Tanaka, 2007a), we use the averaged similarity index $ASI(\tau)$ of the function of τ, which is given by

$$ASI(\tau) = \frac{1}{T} \sum_{t=0}^{T} \frac{\sum_{i=1}^{N} z_i(t) z_i(t+\tau)}{\sqrt{\sum_{i=1}^{N} z_i^2(t)} \sqrt{\sum_{i=1}^{N} z_i^2(t+\tau)}}. \tag{3.6}$$

The right-hand side of this equation represents the extent to which two populations of active neurons at different times with interval τ are correlated. If $ASI(\tau)$ takes a value of

1, the populations at times t and $t+\tau$ are identical, and when $ASI(\tau)$ takes a value of 0, different populations are active at times t and $t+\tau$. The monotonic decrease in $ASI(\tau)$ with increasing $|\tau|$ indicates that the population of active neurons changes with time without recurrence (Yamazaki and Tanaka, 2005). In addition, we also define another index that measures the ability of POT representation. The ideal POT representation is achieved by monotonically decreasing $ASI(\tau)$ with respect to $|\tau|$ with a large difference between $ASI(0)$ and the minimum of $ASI(\tau)$ (Yamazaki and Tanaka, 2007a). However, even in the cases of oscillatory activities overlaid on the random repetition of burst and silent activities, if the temporal coherence of the oscillation decreases with increasing τ, the POT representation is possible to some extent. To extract a residual POT-representing component of the active neurons' population, we first fitted $ASI(\tau)$ with a Gaussian function and calculated the height between $ASI(0)$ and the minimum of $ASI(\tau)$. The height was then divided by 0.376, which is the largest value of the height among all similarity indices examined by a brute-force search varying Mg^{2+} concentration ($[Mg^{2+}]$) and input current strength. We call this normalized height the POT-representation index (PI).

When ith grc elicits spike activity at time t in response to injected current I^{MF}, $f^{(I^{\mathrm{MF}})}(t) = 1$, and otherwise, $f^{(I^{\mathrm{MF}})}(t) = 0$. We define similarity index (SI) as follows:

$$SI(t_1, t_2) = \frac{\sum_{i=1}^{N} f_i^{I_1^{\mathrm{MF}}}(t_1) f_i^{I_2^{\mathrm{MF}}}(t_2)}{\sqrt{\sum_{i=1}^{N} [f_i^{I_1^{\mathrm{MF}}}(t_1)]^2} \sqrt{\sum_{i=1}^{N} [f_i^{I_2^{\mathrm{MF}}}(t_2)]^2}}, \tag{3.7}$$

which represents correlation of a spiking grc population at time t_1 for CS current I_1^{MF} and that at time t_2 for CS current I_2^{MF}. $SI(t_1, t_2) = 1$ indcates that active grc populations at t_1 and t_2 are identical, where $SI(t_1, t_2) = 0$ indicates that completely different grcs elicit spikes at t_1 and t_2.

3.3 Reproducibility Index

To examine the reproducibility of active neurons' population among different trials of the same CS stimulation, we used the previously introduced reproducibility index $RI(t)$ (Yamazaki and Tanaka, 2007a, 2005), given by

$$RI(t) = \frac{\sum_{i=1}^{N} z_i^{(1)}(t) z_i^{(2)}(t)}{\sqrt{\sum_{i=1}^{N} \left[z_i^{(1)}(t) \right]^2} \sqrt{\sum_{i=1}^{N} \left[z_i^{(2)}(t) \right]^2}}. \tag{3.8}$$

Here, the superscripts (1) and (2) indicate two different trials. $RI(t)$ represents the similarity between the populations of active neurons at time t measured from the CS onset in two different trials. When $RI(t)$ takes a value of 1, the populations of active neurons in the two trials are identical, and when it takes a value of 0, they are completely different (Yamazaki and Tanaka, 2007a).

Part I

Sate transition between synchronized oscillation and repetitive bust-silent alternation

Chapter 4

State transition

4.1 Introduction

The cerebellar granular layer is one of the stations receiving external stimuli for information processing of the cerebellar cortex. The granular layer is thought to transform spatial patterns of mossy fibers (MFs) input signals into a population of active granule cells (grcs) (Marr, 1969; Albus, 1971). Recently, Yamazaki and Tanaka (2007a) have proposed that the granular layer transforms spatiotemporal patterns of MF input signals into a sparse population of active grcs in the presence of inhibitory Golgi cells (Gocs), and suggested that the passage of time (POT) from the onset of MF signals is represented by the granular layer network.

In Pavlovian delay eyeblink conditioning (for a review, e.g., Mauk and Donegan, 1997; Hesslow and Yeo, 2002; Christian and Thompson, 2003), an animal is exposed to the paired presentation of a sustained tone (conditioned stimulus: CS) and an airpuff (unconditioned stimulus: US) that induces the eyeblink reflex (Figure 2.1). After the repeated conditioning of CS-US presentation with a fixed interstimulus interval (ISI) between the onsets of the CS and US, the CS presentation alone causes the subject to close the eye as a conditioned response (CR) slightly prior to the US onset timing. This phenomenon indicates that the subject memorizes the ISI. Several researchers have hypothesized that the POT from the CS onset is encoded by the sequential activation of grc populations (for a review, see Yamazaki and Tanaka, 2009).

On the other hand, when an animal stays at rest without any external stimuli, oscillatory local field potential (LFP) is observed in the granular layer at 7–8 Hz in rats (Hartmann and Bower, 1998) and at 13–14 Hz in monkeys (Pellerin and Lamarre, 1997; Courtemanche et al., 2009). Although the origin of this oscillation remains unknown, Maex and De Schutter (1998) proposed that grcs and Gocs become active alternatingly and repeated by the recurrent connections, and their average oscillatory firing may be observed as the oscillation of LFP.

There are two distinct dynamics in the cerebellar granular layer: one for the POT representation and the other for the synchronized oscillation. Assuming that the two dynamics emerge from the same neural circuits, one may expect that the presence or absence of the CS controls the transition between the two dynamics. However, models accounting for the POT representation do not exhibit the synchronized oscillatory firing of grcs and Gocs but generates spikes randomly in the absence of the CS (Yamazaki and Tanaka, 2007a), whereas models accounting for the synchronized oscillation persistently show the oscillatory state even in presence of the CS (Maex and De Schutter, 1998). Therefore, it is not trivial to explain the two dynamics in the same model of the cerebellar granular layer.

In this study, we rebuild a spiking network model of the cerebellar granular layer, which represents the POT in response to the CS and generates the synchronized oscillatory firing of grcs and Gocs when the CS is not presented.

4.2 Stimulus and simulation paradigm

We model MF input signals as current injected directly to the soma of each model grc, instead of spike trains. Freeman and Muckler (2003) have reported that the spontaneous firing rate of MFs is as low as 5 Hz, whereas the firing rate increases up to 30 Hz when an animal is stimulated with a tone (e.g., CS). We assume that the current injected into grcs increases with the frequency of firing conveyed through MFs. In the simulation, we inject a current I_{MF} of 10.7 pA to all model grcs for 2 s to simulate grc activity induced by spontaneous MF activity. For the succeeding 2 s, we inject a current I_{MF} of 22.7 pA to evoke activity in grcs in response to high-frequency MF firing induced by the presentation of the

CS. Subsequently, we inject a current I_{MF} of 10.7 pA for 2 s again to resume the baseline activity of grcs induced by the spontaneous MF activity. In total, we simulate the dynamics of the granular layer network for 6 s. Note that we omit noise in the current injected to grcs in order to stress that randomness in grc activities relevant to POT representation is intrinsically generated by the network structure but not due to noisy current.

4.3 Results

4.3.1 Input-dependent transition of dynamical states in the model granular layer

Figures 4.1B and C represent the temporal patterns of spikes generated by 200 representative model Gocs and grcs, respectively, in response to the injection of current to the grcs (Figure 4.1A). For the first 2 s, in which a small current was fed to the grcs, simulating a response to spontaneous MF activity, model grcs and Gocs elicited spikes rhythmically and synchronously with a frequency of 9 Hz. The emergence of the synchronized oscillation in the grcs and Gocs is consistent with the findings of Maex and De Schutter (1998). For the successive 2 s, in which a CS signal was presented to the grcs by injecting a large current, the model grcs exhibited random alternation between the burst and silent modes, consistent with the findings of Yamazaki and Tanaka (2007a). After the cessation of the CS presentation, the network quickly returned to the oscillatory state at 9 Hz. These simulation results show that the model cerebellar granular layer can exhibit two qualitatively distinct dynamical states depending on the strength of the MF input signal. In the following subsections, we examine the properties of each dynamical state in detail.

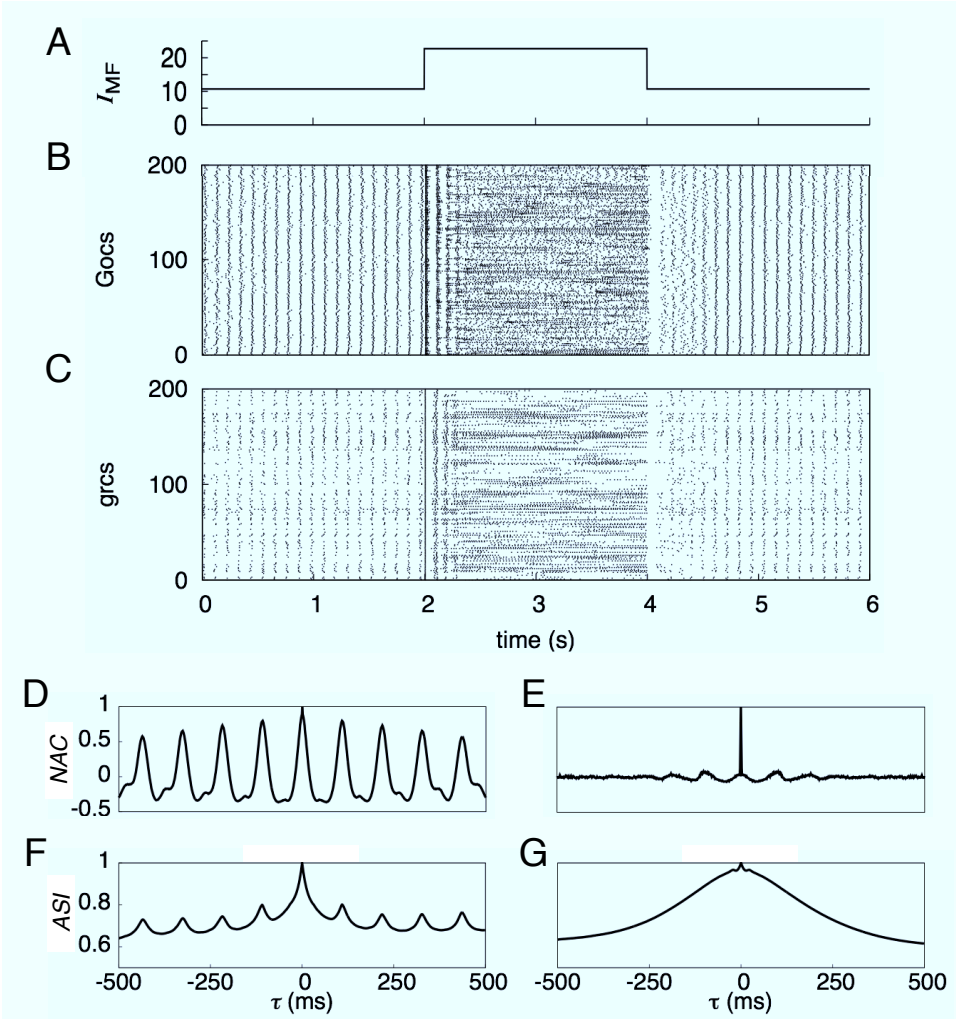

Figure 4.1: Activities of grcs and Gocs in response to current injected to model grcs. A, Temporal pattern of injected current, in which a small current was injected for 0–2 and 4–6 s, whereas a large current was injected for 2–4 s. B and C, Spike patterns of 200 out of 1024 grcs and 200 Gocs, respectively. During the injection of a small current, grcs and Gocs elicited spikes synchronously and rhythmically. During the injection of a large current, the populations of active grcs and Gocs exhibited random alternation between the burst and silent modes. D and E, Normalized autocorrelation functions, $NAC(\tau)$, during the injection of small and large currents, respectively. F and G, Similarity index functions, $ASI(\tau)$, of grcs are shown during small and large current injections, respectively. $NAC(\tau)$ indicates the oscillatory generation of spikes and $ASI(\tau)$ shows that similar spike patterns were repeatedly generated, although the spike patterns gradually became different gradually with the separation of time during the small current injection. On the other hand, during the large current injection, $NAC(\tau)$ indicates the random spike generation and $ASI(\tau)$ shows that the spike pattern changed gradually and that each pattern was only generated once.

4.3.2 Synchronized oscillation generated by MF spontaneous activity

To confirm the generation of synchronized oscillation at model grcs in response to spontaneous MF activity (0–2 s), we calculated a normalized autocorrelation function $NAC(\tau)$ of the activities of the grcs using Equation 3 and the value of the oscillation index OI using Equation 4. We found a clear oscillation at 9 Hz, as shown in Figure 4.1D. We also obtained $OI = 0.836$, suggesting robust synchronization of the activities of the model grcs, and observed the synchronized oscillation at 9 Hz from 4 to 6 s. This oscillation frequency was in the range of oscillation frequencies of cerebellar LFP observed by Hartmann and Bower (1998) and Pellerin and Lamarre (1997) (7–8 Hz in rats and 13–14 Hz in monkeys). This frequency became lower than that shown by Maex and De Schutter (1998) due to a larger decay constant of γ-aminobutyric acid-A receptor ($GABA_AR$)-mediated IPSPs on model grcs. These results suggest that the granular layer of the biological cerebellum is in a state of synchronized oscillation in the absence of the CS signal input. The similarity between spike activity patterns at different times decreased with the time interval, but patterns showed weak oscillation associated with synchronized oscillation (Figure 4.1F). The $NAC(\tau)$ and similarity index $ASI(\tau)$ for model Gocs were similar to those for model grcs (Figure 4.2).

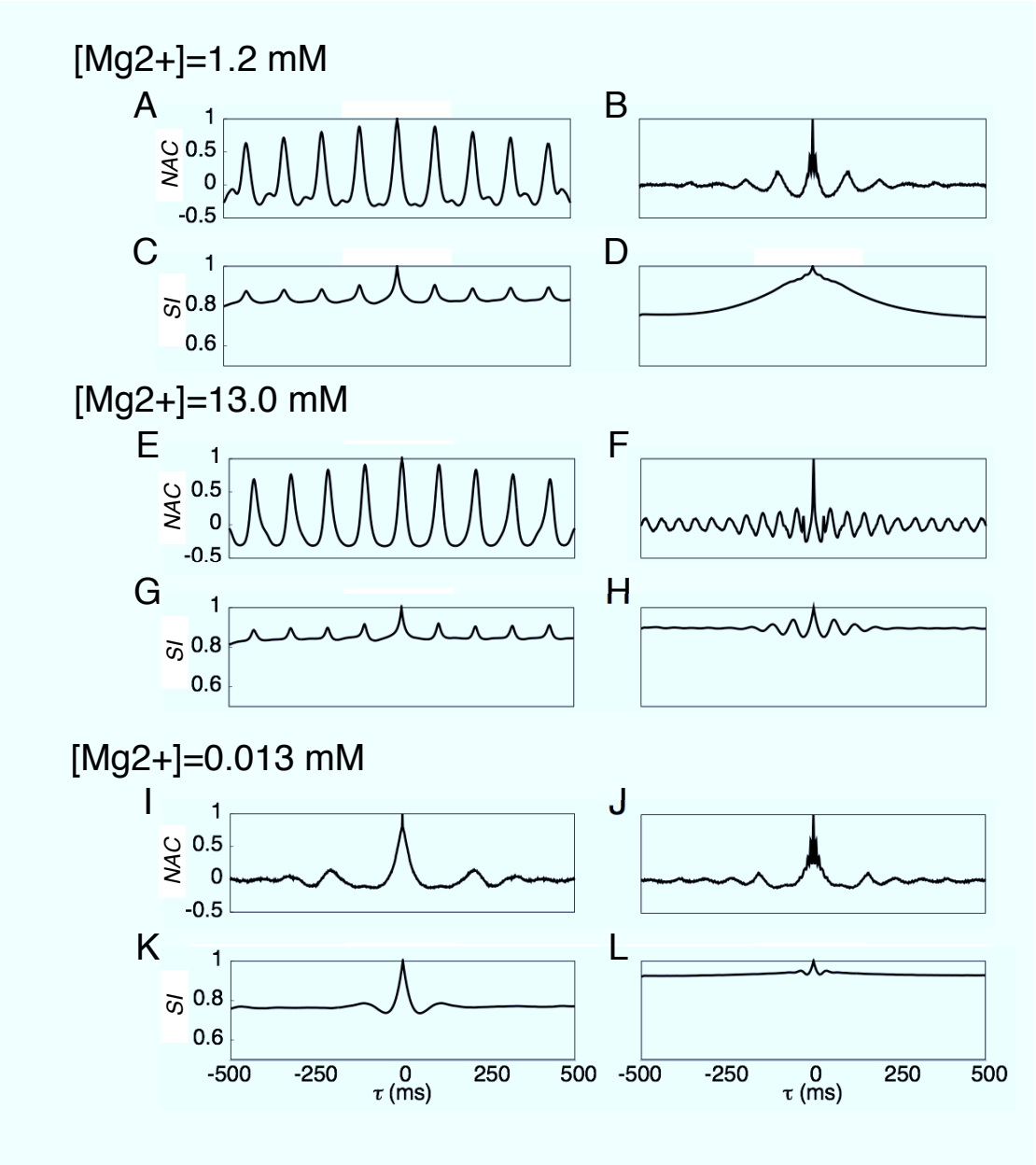

Figure 4.2: Normalized autocorrelation functions (A, B, E, F, I and J) and similarity indices (C, D, G, H, K and L) of Goc spike activities for different conditions. The left column (A, C, E, G, I and K) was calculated from Goc spike activities when a small current was injected to the grcs, whereas the right column (B, D, F, H, J and L) was calculated when a large current was injected. A–D, E–H and I–L were calculated from Goc activities at default, high and low values of $[Mg^{2+}]$, respectively.

The emergence of synchronized oscillation may be interpreted in terms of the following circuit mechanism between grcs and Gocs. The relatively low average firing rate of grcs induced by a small input current evokes the weak depolarization of Gocs, which rarely opens voltage-gated NMDA channels on the Goc dendrites. Thereby, the Gocs elicit only single spikes followed by a refractory period. The low-frequency spike activity of the Gocs inhibits grcs, which become inactive. After the recovery from the inhibition due the Gocs, the grcs become active due to the sustained external current input, and elicit low frequency spikes. The repetition of such activation and deactivation processes results in the synchronized oscillation of the model grcs and Gocs. This mechanism for the emergence of the oscillatory state is the same as that reported by Maex and De Schutter (1998).

The average firing rate of individual grcs was less than half ($\approx$ 4 spikes/s) of the oscillation frequency (9 Hz) in our simulations. This indicates that not all grcs were activated at every oscillation cycle, which is attributed to the random and sparse connectivity between the Gocs and grcs. When the inhibition of the grcs by the Gocs was removed, the grc firing rate increased to 44 spikes/s. This result suggests that the oscillation frequency was determined by the network dynamics, rather than the mechanisms of individual grcs firing driven by the noise-free current input.

4.3.3 POT representation by CS-evoked MF activity

Figures 4.1B and C also represent spike patterns of 200 model Gocs and grcs, respectively, in response to the injection of a large current to the grcs, which are induced by the CS input through MFs in the interval from 2 to 4 s. Model grcs clearly exhibited random alternation between the burst and silent modes. Therefore, the normalized autocorrelation $NAC(\tau)$ is markedly reduced except at $\tau = 0$ ms (Figure 4.1E). Different grcs showed different patterns of spike trains. To determine whether the same active grc populations appear more than once, we calculated the similarity index $ASI(\tau)$ using Equation 6 and plotted it in Figure 4.1G. The value of $ASI(\tau)$ was 1 at $\tau = 0$ ms because of the trivial identity. $ASI(\tau)$ monotonically decreased as $|\tau|$ increased with the POT-representation index $PI = 0.923$. This indicates that the population of active grcs changed gradually with time from the CS onset without the recurrence of active grc populations, as reported by Yamazaki and Tanaka

(2007a). The $NAC(\tau)$ and $ASI(\tau)$ for model Gocs were similar to those for model grcs (Figure 4.2). To determine the effect of random connections between model grcs and Gocs, we performed simulations using a modified model in which grcs and Gocs were all connected with each other so that the network did not have any randomness. As a result, activities of these cells exhibited only coherent oscillations (Figure 4.3). This suggests that the random connectivity is a major cause of generating the random alternation between burst and silent modes in grcs and Gocs. The nonrecurrence of active grc populations implies a one-to-one correspondence between a certain population of active grcs and a certain time during the large current injection. Thus, the sequence of active grc populations can represent the POT from the CS onset.

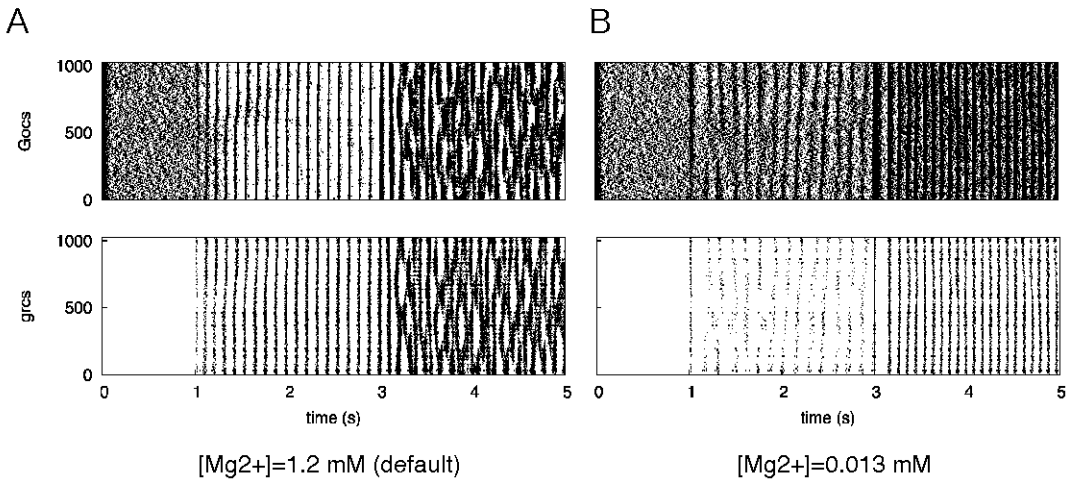

Figure 4.3: Raster plots of grcs (upper panel) and Gocs (bottom panel) when connection probabilities between grcs and Gocs are 1.0. A and B show $[Mg^{2+}]$ is 1.2 mM (default case) and 0.013 mM ($[Mg^{2+}]$-free condition).

The random alternation between the burst mode and the silent mode of grcs can be accounted for by the following dynamics in the granular layer. The strong activation of grcs by the CS presentation vigorously depolarizes randomly connected Gocs, resulting in the activation of voltage-gated NMDA channels on the dendrites of the Gocs. Because of the long decay time constant of NMDAR-mediated EPSPs, Gocs send sustained inhibitory signals to nearby grcs, so that the grcs become inactive. Then a Goc that receives inputs

from these grcs decreases its activity, which reactivates the grcs. However, due to the random connections, the timings of the reactivation and deactivation of grcs are different for different grcs, resulting in the random alternation between the burst and silent modes of grcs.

4.3.4 Reproducibility of POT-representing states in grc populations

To realize robust and reproducible POT representation for different trials of CS presentation, almost the same sequence of active grc populations must appear in response to the same CS, even if the initial network states are different. To confirm that the present model shows such reproducibility, we carried out the following simulations. We injected a large current to grcs, corresponding to a CS signal input through MFs, twice during 2–4 and 6–8 s, whereas we injected a small current, corresponding to spontaneous firing of MFs, at other times. We evaluated the value of the reproducibility index $RI(t)$ between active grc populations in response to the first injection of a large current and those in response to the second injection of a large current using Equation 7 (Figure 4.4). The reproducibility between the two active grc populations immediately after the CS onsets was high, but it tended to decrease with the duration of large current injection. The large $RI(t)$ observed immediately after the CS onset was attributed to the simultaneous activation of all grcs and Gocs, which served to reset the network state. This resetting at the CS onset enables the network to lose its history of activities, which guarantees that the network dynamics during large current injection is reproducible independently of the initial states in the granular layer. Consequently, the present model can represent the POT robustly and reproducibly for different trials of CS presentation.

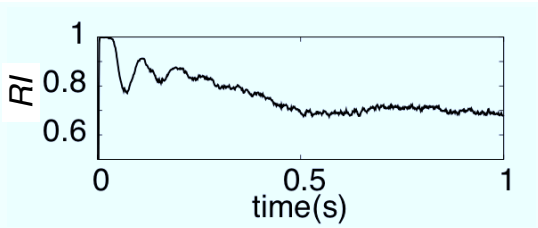

Figure 4.4: Reproducibility of spike patterns of grcs for injection of a large injection.

4.3.5 Effects of Mg^{2+} concentration on POT representation

To confirm the importance of NMDA channels expressed on the dendrites of model Gocs for POT representation, we blocked the channels by increasing the concentration of Mg^{2+} (1.20 mM $\rightarrow$ 13.0 mM) and carried out a simulation.

Figure 4.5 shows spike trains elicited by 200 Gocs (Figure 4.5B) and 200 grcs (Figure 4.5C) in response to current injection (Figure 4.5A) under the blockade of the NMDA channels on the model Gocs. The synchronized oscillation of grcs and Gocs was unaffected during the injection of a small current to the grcs for 0–2 and 4–6 s, which corresponds to the input of spontaneous MF activities. This was observed by the appearance of oscillatory behavior of the normalized autocorrelation function $NAC(\tau)$ (Figure 4.5D). The similarity index $ASI(\tau)$ was similar to that in the default case (Figure 4.5F). As mentioned previously, when the input stimulus was weak, the NMDA channels on the Goc dendrites rarely opened, irrespective of whether or not NMDA channels were blocked, because of the voltage dependence of the channels. Therefore, it is considered that the blockade of NMDA channels did not change the network dynamics during small current injections. On the other hand, in response to a large current injection to the grcs for 2–4 s, which corresponds to CS presentation, the grcs elicited spikes at a higher firing rate than in the default case (13 spikes/s $\rightarrow$ 32 spikes/s) and the spike patterns were random and uniform, as can be seen in Figure 4.5C. This observation was justified by the fact that $NAC(\tau)$ showed oscillation whose amplitude was sufficiently small compared with its value at $\tau = 0$ (Figure 4.5E). The grcs did not show random alternation between the burst and silent modes. This was caused by the weaker inhibition from Gocs due to the blockade of NMDA channels. As shown in Figure 4.5G, $ASI(\tau)$ became much higher than in the default case. The POT-representation index PI was as small as 0.009, compared with the value of 0.923 in the default case. This indicates that the temporal sequence of active grc populations does not represent the POT even during a large current injection. We confirmed similar tendency for the activity patterns of model Gocs (Figure 4.2).

Taken together, the activation of NMDARs on the Goc dendrites is not important for the generation of synchronized oscillation of grc and Goc activities. In contrast, the activation of the NMDARs is indispensable for the generation of active grc populations

randomly alternation between the burst and silent modes, which enables the network to represent the POT.

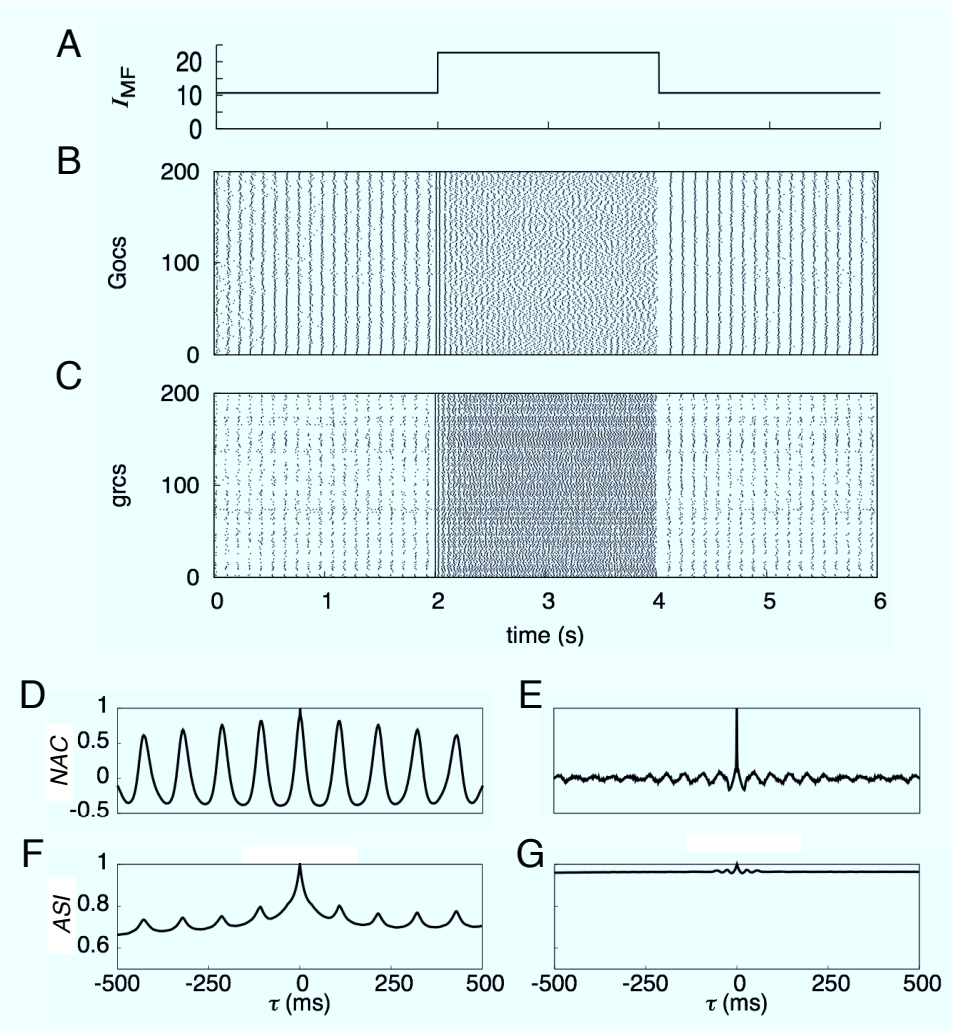

Figure 4.5: Activities of model grcs and Gocs when NMDA channels of model Gocs were blocked. Conventions are as in Figure 4.1. B and C show that the grcs and Gocs elicited spikes synchronously and rhythmically during the small current injection, and that they generated spikes randomly during the large current injection. Even for the blockade of NMDA channels, the statistical features of the activity patterns of grcs during the small current injection (D and F) were the same as those shown in Figures 4.1D and F. When a large current was injected, the sufficiently small amplitude of oscillation in $NAC(\tau)$ shown in E indicates that grcs elicited spikes randomly, and the constant $ASI(\tau)$ shown in G indicates that active grc populations were almost the same.

4.3.6 Effects of Mg^{2+} concentration on the oscillatory states

Next, to examine whether the oscillatory states are affected by the reduced Mg^{2+} concentration, we performed a simulation under a nearly [Mg^{2+}]-free condition (0.013 mM).

Figures 4.6B and C show spike trains of 200 model Gocs and grcs, respectively, in response to the current injection to the grcs (Figure 4.6A). The spike trains of the grcs exhibited random alternation between the burst and silent modes in response to a large current injection for 2–4 s. The observation of randomness in the spike activity patterns was justified by the fact that the normalized autocorrelation function $NAC(\tau)$ took almost zero except at $\tau = 0$ (Figure 4.6E). Although the firing rate of the grcs was reduced by the enhanced inhibition from the Gocs, the similarity index $ASI(\tau)$ decreased monotonically with τ (Figure 4.6G), as seen in the case where the POT is represented. On the other hand, for 0–2 and 4–6 s, during which a small current was injected, the grcs and Gocs did not undergo synchronized oscillation (Figure 4.6D). The grcs generated spikes sparsely in a stochastic manner (the oscillation index $OI = 0.207$), whereas the Gocs elicited spikes at almost the same frequency as that in the default setting. $ASI(\tau)$ monotonically decreased due to the absence of synchronized oscillation (Figure 4.6F). These results indicate that the persistent reduction of Mg^{2+} concentration from NMDA channels on the Goc dendrites disrupts the synchronized oscillation. We confirmed similar tendency for the activity patterns of model Gocs (Figure 4.2).

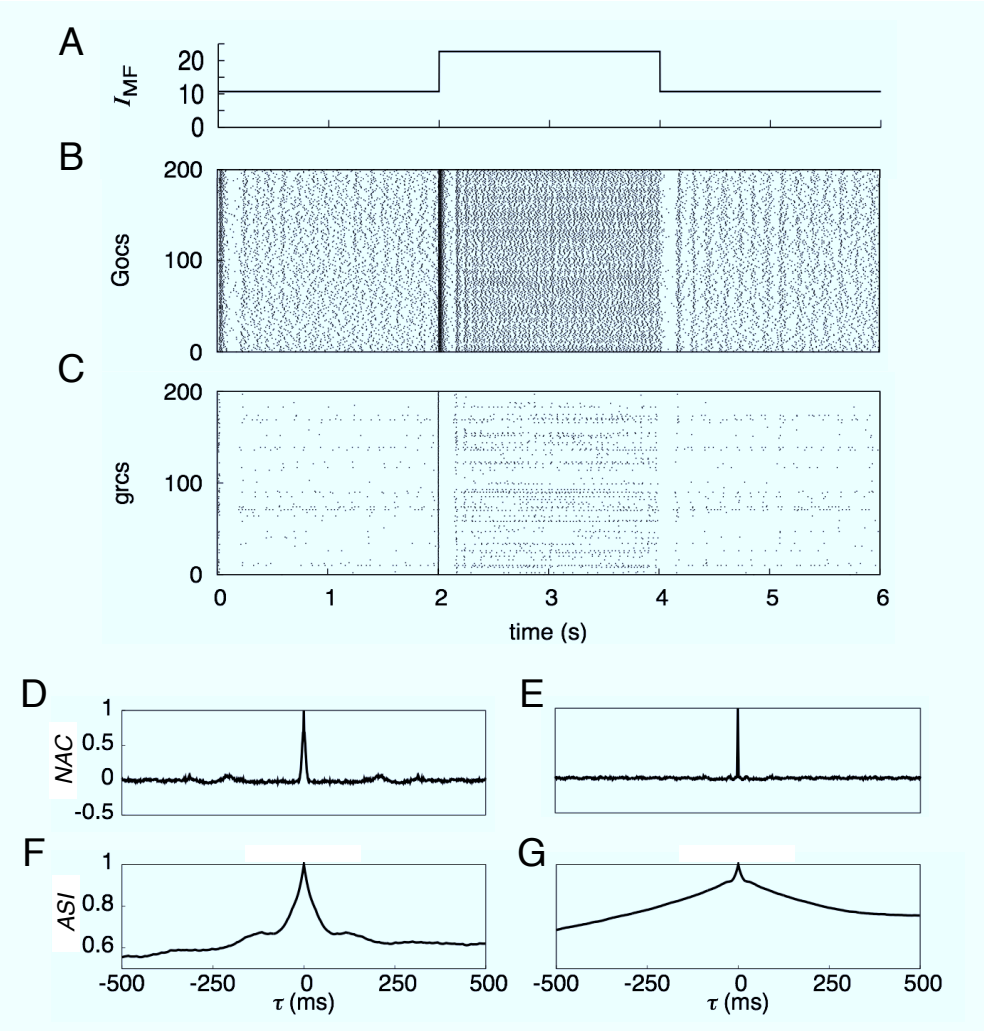

Figure 4.6: Activities of grcs and Gocs when NMDA channels of Gocs were continually open. Conventions are as in Figure 4.1. B and C, Spike patterns of 200 grcs and 200 Gocs, respectively. When a small current was injected, the Gocs elicited spikes at high frequencies (B), which in turn strongly inhibited the grcs. Consequently, the generation of oscillatory spikes by grcs disappeared (C). The absence of the oscillation was demonstrated by the sharp peak of $NAC(\tau)$ at $\tau = 0$ (D). The overlap of active grc populations decreased rapidly with the separation of time (F). When a large current was injected, the Gocs also fired at high frequencies, too (B). In this case, however, the populations of active grcs exhibited random alternation between the burst and silent modes although the grcs elicited spikes sparsely (C, compared with Figure 4.1C). This random spike pattern was demonstrated by the sharply localized peak of $NAC(\tau)$ at $\tau = 0$ and otherwise, $NAC(\tau) \approx 0$, as shown in E. $ASI(\tau)$ monotonically decreased as $|\tau|$ increased (G), indicating that the population of active grcs changed gradually to different populations with time without recurrence.

4.3.7 Various dynamical states generated by the control of Mg^{2+} concentration

Here we examine how the network dynamics changes depending on the Mg^{2+} concentration.

Figure 4.7A shows the changes of the oscillation index *OI* and POT-representation index *PI* with $[Mg^{2+}]$. For $[Mg^{2+}]$ in the interval between 0.013 mM and 0.260 mM, *PI* was almost constant at around 0.510. As $[Mg^{2+}]$ increased beyond 0.260 mM, *PI* decreased and reached 0.146 at $[Mg^{2+}] = 0.469$ mM. Then, *PI* started to increase and reached a maximum at $[Mg^{2+}] = 1.40$ mM. As $[Mg^{2+}]$ increased further, the *PI* decreased again and vanished for $[Mg^{2+}] > 6.52$ mM. The POT-representing states emerged only when $[Mg^{2+}]$ was between 0.782 and 2.45 mM. *OI* was high in two separate domains where $[Mg^{2+}]$ was in the intervals of 0.417 mM and 0.782 mM, and 5.21 mM and 9.13 mM. Hence, the domain where the POT representing state appeared was sandwiched by two high-*OI* domains.

Figure 4.7B shows the firing rate and oscillation frequency averaged over all the model grcs. The average oscillation frequency gradually decreased from 12 to 7 Hz as $[Mg^{2+}]$ increased from 0.0130 to 0.834 mM. As $[Mg^{2+}]$ increased beyond 0.834 mM, the frequency increased in turn and saturated at 22 Hz. Therefore, the average oscillation frequencies in the two high-*OI* domains were 7–8 and 20–21 Hz. In contrast, the firing rate monotonically increased from 5 to 32 spikes/s as $[Mg^{2+}]$ increased.

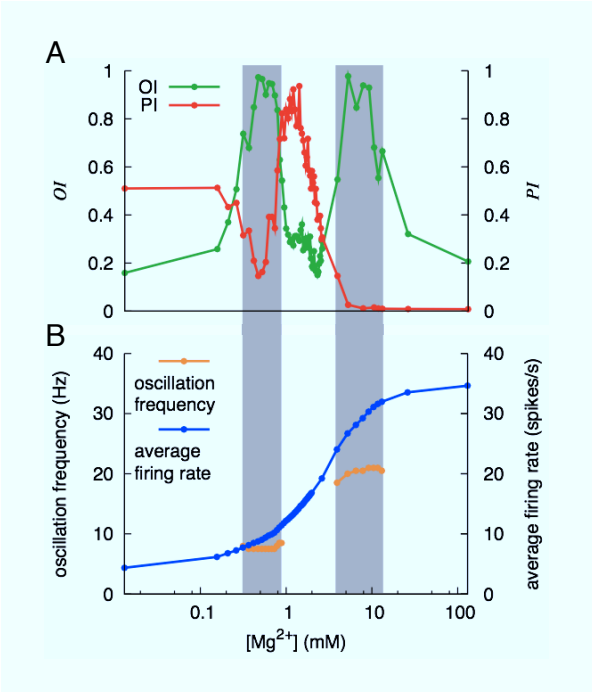

Figure 4.7: Dynamical states of the network during current injection ($I_{\mathrm{MF}} = 22.7$ pA) with various concentrations of Mg^{2+}. A, Dependence of the oscillation index (OI) and POT representation index (PI) on the concentration of Mg^{2+}. OI was large in two separate regions of Mg^{2+} concentration, which are indicated by the vertical gray bands. In-between these gray bands, there is a domain in which PI was larger than 0.5. B, Average firing rate of grcs and frequency of oscillatory spike generation. The average firing rate increased monotonically as the Mg^{2+} concentration increased. The oscillation frequency was around 7 Hz within the interval of 0.417–0.782 μM and around 20 Hz within the interval of 5.21–9.13 μM.

4.3.8 Distinct dynamical states generated by controlling the strength of injected current

Next, we analyzed the transition of activity patterns as we changed continuously the strength of the injected current. Figure 4.8A shows the changes of the oscillation index OI and POT-representation index PI with the strength of the injected current to the grcs, I_{MF}. When I_{MF} was less than 6.5 pA it was too small for the grcs to be activated,

and hence PI could not be defined at $I_{\mathrm{MF}} < 6.5$ pA. For I_{MF} between 6.5 pA and 16.5 pA, there was a local maximum of PI ($PI = 0.269$) at $I_{\mathrm{MF}} = 8.0$ pA. PI exhibited a maximum at around $I_{\mathrm{MF}} = 26.5$ pA. For $I_{\mathrm{MF}} > 26.5$ pA, PI gradually decreased as I_{MF} increased. POT representing states were well defined when I_{MF} was between 19 pA and 33 pA. On the other hand, synchronized oscillation states were well defined in the interval of I_{MF} between 9.5 pA and 18 pA, whereas OI remained low values outside this interval.

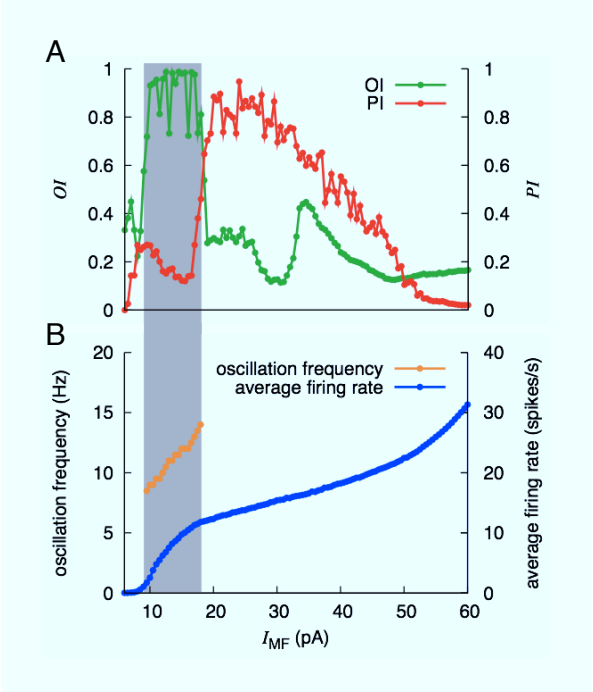

Figure 4.8: Dynamical states of the network for various amplitudes of the injected current at $[Mg^{2+}] = 1.2$ mM. A, I_{MF} dependence of OI and PI. High value of OI and PI tended to appear complementarily along the I_{MF} axis: OI was larger at a smaller current, whereas PI was larger at a larger current. B, I_{MF} dependence of average firing rate and oscillation frequency of grcs. The average firing rate increased monotonically as I_{MF} increased. The oscillation frequency linearly increased from 9 to 14 Hz as I_{MF} increased from 9.5 to 18 pA within the high OI domain.

Figure 4.8B shows the average firing rate and the oscillation frequency of grcs against the strength of the injected current. The oscillation frequency is shown for the range of the injected current in which oscillation states are well defined. The oscillation frequency

was dissociated from the average firing rate. As I_{MF} increased, the firing rate gradually increased from 0 to 31 spikes/s. Beyond $I_{\mathrm{MF}} = 50$ pA, it showed a relatively rapid increase.

4.3.9 State transition in the parameter space spanning Mg^{2+} concentration and input stimulus strength

Here, we explore all possible dynamical states in the present network model by varying the values of $[Mg^{2+}]$ and I_{MF} exhaustively. Figure 4.9 shows the values of the oscillation index OI and POT-representation index PI of grc spike patterns in green (Figure 4.10A) and red (Figure 4.10B), respectively. In Figure 4.11, we show the spike trains, similarity indices and normalized autocorrelation functions of the network dynamics at eight representative points marked by asterisks in the state map in Figure 4.9. Point 1 is characterized by an extremely high firing rate of grcs without oscillations. Point 1 corresponds to the case of a strong blockade of NMDA channels on Goc dendrites. Because of the weaker inhibition of grcs by Gocs than the excitation of grcs by the injected current, both PI and OI had small values ($PI = 0.075$ and $OI = 0.133$), while the average firing rate was high (38.4 spikes/s) (Figures 4.9 and 4.10D). Point 2 exhibits synchronized oscillation induced by a small injected current. The PI, OI and the oscillation frequency at point 2 were 0.052, 0.991 and 13 Hz, respectively. Points 1 and 2 are irrelevant to the POT representation. Points 3 and 6 are closely related to the POT representation. In particular, point 3 corresponds to a typical POT-representing state, at which PI and OI were 0.943 and 0.159, respectively. Also at point 6, the grcs showed a POT-representing state due to the sustained opening of the NMDA channels at the Gocs at a low $[Mg^{2+}]$. However, PI was lower than that at point 3 ($PI = 0.580$ and $OI = 0.243$). Point 4 appears to be located at the transition from synchronized oscillation to POT representation, because synchronized oscillation appeared transiently and changed to POT-representing states, as observed at points 3 and 6. The synchronized oscillation collapses with a long relaxation time. This weak synchronized oscillation became stronger with decreasing I_{MF}, as can be seen at point 5 (oscillation frequency = 7 Hz; $OI = 0.969$ (Figures 4.10C) and 4.11), which was caused by the repeated bumping of strong excitation of Gocs mediated by NMDA channels. The lower firing rate of the grcs at point 7 was caused by strong inhibition from the Gocs,

which exceeded the excitation due to the large current injected to the grcs. Finally, point 8 corresponds to almost inactive states of the grcs exhibiting neither synchronized oscillation nor POT representation due to too weak MF input signals or strong inhibition from Gocs, at which the NMDA channels were persistently open.

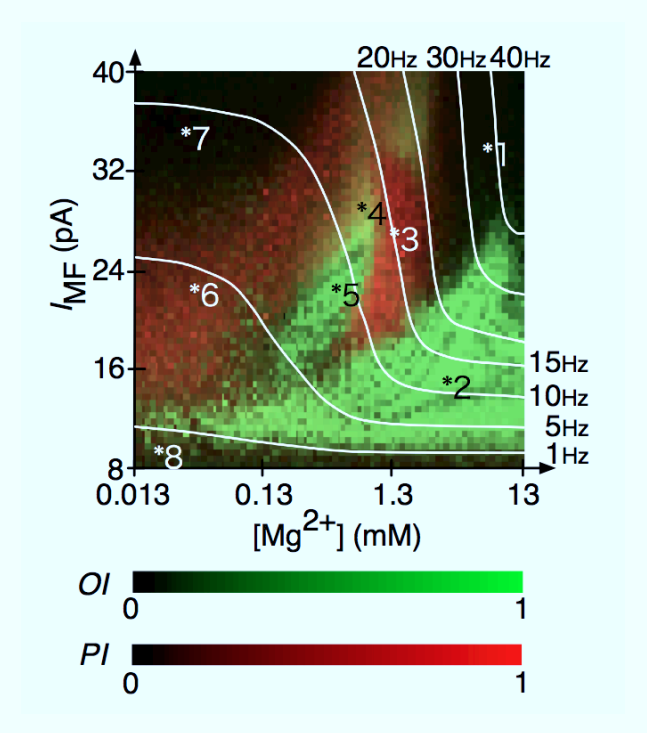

Figure 4.9: *OI* and *PI* for the present model in the space spanned by $[Mg^{2+}]$ and I_{MF}. The abscissa and ordinate represent $[Mg^{2+}]$ and I_{MF}, respectively. Values of *OI* are shown in the brightness of the green color, where the darkest shade indicates $OI = 0$ and brightest shade indicates $OI = 1$. Values of *PI* are shown by the brightness of the red color such that the darkest shade indicates $PI = 0$ and the brightest shade indicates $PI = 1$. Greenish or reddish domains indicate that the network exhibited synchronized oscillatory states or POT-representing states, respectively. Eight typical points are picked out from this parameter space. The white lines represent average firing rates of grcs of 1, 5, 10, 15, 20, 30 and 40 Hz.

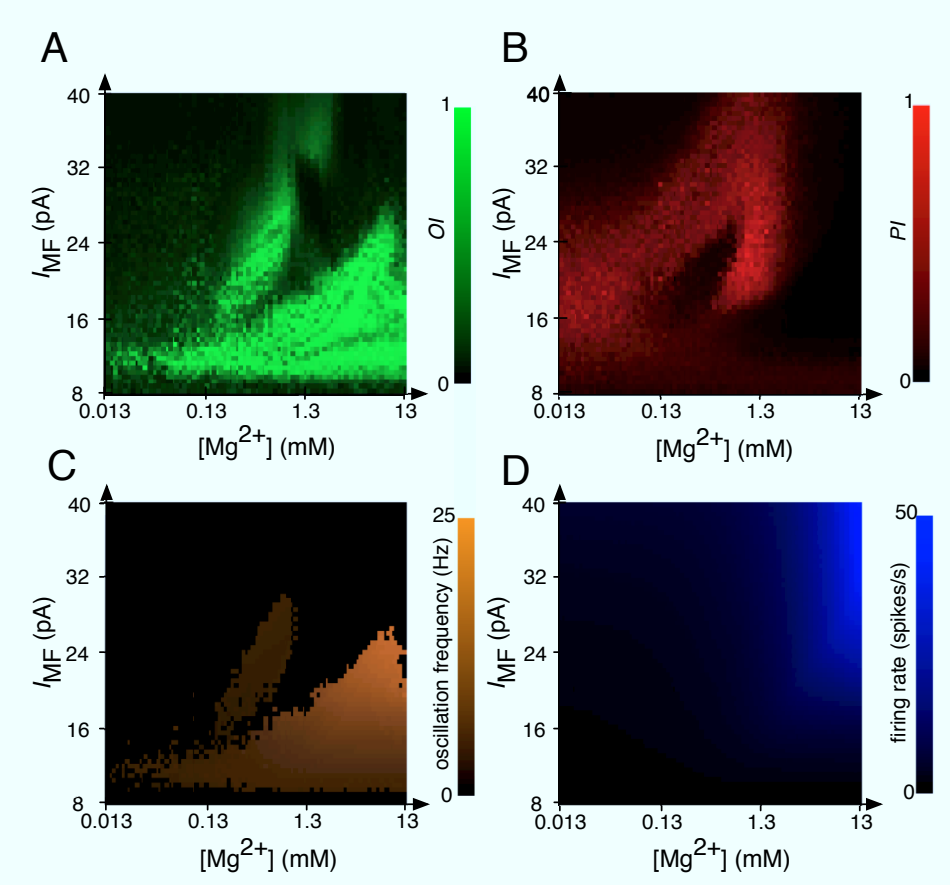

Figure 4.10: Network behaviors in the parameter space spanned by [Mg^{2+}] and I_{MF}. The oscillation index (A) and POT-representation index (B), which characterize the network dynamics, are plotted in the parameter space with different colors. Figure 4.9 was obtained by overlapping A and B. The frequency of oscillatory spike generation (C) and average firing rate of grcs (D). The average firing rate increased monotonically as the Mg^{2+} concentration or I_{MF} increased. The oscillation frequency was constantly around 7 Hz at the center of (C).

We can classify the eight points into four different states: a synchronized oscillation state (State I), POT-representing state (State II), a metastable state (State III) and a uniform firing state (State IV). State I to IV are represented by the dynamical states at points 2 and 5, points 3 and 6, point 4 and points 1, 7 and 8, respectively. State II is observed when the average firing rate of the grcs is approximately 1–20 Hz (Figure 4.9B).

When $[Mg^{2+}]$ was approximately 1.0–1.5 mM and I_{MF} was 22–33 pA, the value of PI was higher and the average grc firing rate was not changed. This shows that the strengths of the excitation and inhibition to grcs are the same in a network with these parameters. Also, even if the average grc firing rate is approximately 1–20 Hz, State I and II can be observed (Figure 4.9B).

Although the state map is convenient for overviewing possible steady states in the dynamics of the model granular layer network, it should be noted that transient dynamics, as shown at point 4 in State III, may be partially engaged in temporal information processing.

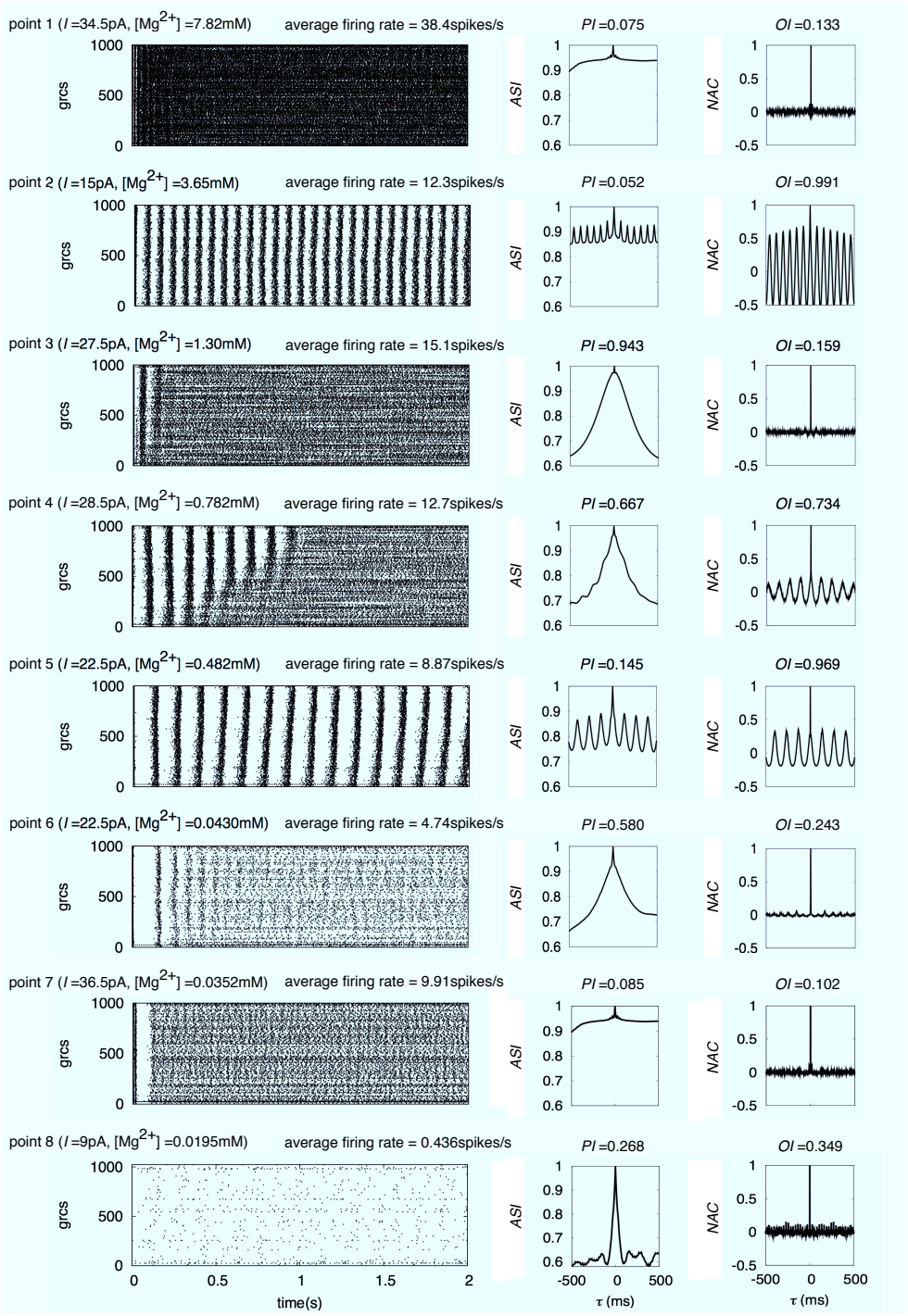

Figure 4.11: Spike patterns, similarity indices and normalized autocorrelation functions at eight points as in Figure 4.9. The average firing rate, *PI* and *OI* are each figure given for each point.

4.3.10 Simulation of delay eyeblink conditioning

Cerebellar model

We conducted simulations of delay eyeblink conditioning to demonstrate that an ISI can be learned. Figure 2.1 illustrates a schematic diagram of the CS and US to the cerebellar cortex during delay eyeblink conditioning. The sustained CS is fed to grcs through MFs, whereas the US is sent to PCs through climbing fibers (CFs) with a certain delay. We employ a Hodgkin-Huxley unit as a model PC assuming that the PC receives excitatory inputs from all PFs (Figure 2.1A). The PF input signals are modeled as APMAR-mediated EPSPs. The decay time constant is set at 30 ms (Llano et al., 1991), and the peak conductance is set so that the model PC elicits spikes at a maximum rate of 100 spikes/s in response to a CS (Kotani et al., 2003).

We assume that the US is fed after either 0.5, 0.75 or 1.0 s from the CS onset and that simulated long-term depression (LTD) is induced when PFs and a CF are coactivated within a brief time window (Ito, 1984). We set initial the synaptic weights of PF_i in the model PC, $w_i^{(0)}$, to 1. When grc i fires 0.05–0.1 s before the onset of a US, w_i is set to 0; otherwise, w_i is not changed. For simplicity, we assume only LTD at PF terminals at a model PC. It is because the purpose of the present study in this capter is to elucidate computational mechanisms for the emergence of synchronized oscillatory states and POT-representing states in the same network model rather than to reproduce details of experimental data such as the extinction or reacquisition of CRs in delay eyeblink conditioning. In this sense, the assumption of only LTD is sufficient to show that the PCs can stop firing at appropriate timing after eyeblink conditioning.

Regarding only 2 values for synaptic weights, we have examined two variant LTD models with different time windows, which were suggested from experimental data. We set initial synaptic weights of PF_i terminated at a model PC, $w_i^{(0)}$, to be 1. Equation 4.1 for synaptic weight changes was obtained from the least square fitting to the experimental data with a Gaussian function (Chen and Thompson, 1995). $t^{(f)}$(ms) indicates the time of an f th spike arriving at the PF_i terminal, t_{US} (ms) represents the time of arrival of a US signal at the PC and Tr is the trial number of conditioning.

$$w_i^{(Tr)} = \begin{cases} w_i^{(Tr-1)} \prod_f (1 - 0.1e^{-\frac{(t^{(f)}-250-t_{\rm us})^2}{2\cdot 89.8^2}}) \\ \qquad\qquad t_{\rm us} - 250 \le t^{(f)} \le t_{\rm us}, \\ w_i^{(Tr-1)} \qquad\quad \text{otherwise.} \end{cases} \tag{4.1}$$

In a similar vein, Equation 4.2 for synaptic weight changes was obtained from the least square fitting to another experimental data with a Gaussian function (Wang et al. 2000).

$$w_i^{(Tr)} = w_i^{(Tr-1)} \prod_f (1 - 0.1e^{-\frac{(t^{(f)}-64.0-t_{\rm us})^2}{2\cdot 79.8^2}}). \tag{4.2}$$

For simplicity, we omitted the contribution of synaptic potential generated by the US through the climbing fiber to an EPSP of the model PC.

Simulation results

We conducted simulations of delay eyeblink conditioning to confirm that the model PC can read out a POT represented by the model granular layer. We embedded a model PC in the model granular layer so that the PC received excitatory inputs from all model grcs.

Figure 4.12 shows the membrane potential of the model PC before and after the simulated conditioning. Before conditioning, the PC continuously elicited spikes at a high frequency during the CS presentation. In the simulated conditioning, the US signal was assumed to be given 0.75 s after the CS onset. The synaptic weights of the active PFs connected to the PC were set to zero 0.05–0.1 s before the US onset, whereas the synaptic weights of the other PFs were unchanged. After the conditioning, the model PC stopped firing about 200 ms earlier than the US onset. Specifically, when the US signal was fed 0.75 s after the CS onset, the PC stopped firing at about 0.53 s after the CS onset and restarted at about 0.91 s. This result indicates that the model PC is able to learn the ISI between the CS and US onsets, which reproduces the experimental result of Jirenhed et al. (2007). We also confirmed that the model PC was able to learn other ISIs by setting the ISI to 0.5 or 1 s (Figure 4.12). When the CS signal was not presented, the model PC elicited burst spikes rhythmically at 9 Hz. This reflected the synchronized oscillation of grcs rather than the oscillation induced by intrinsic cellular mechanisms of the PC.

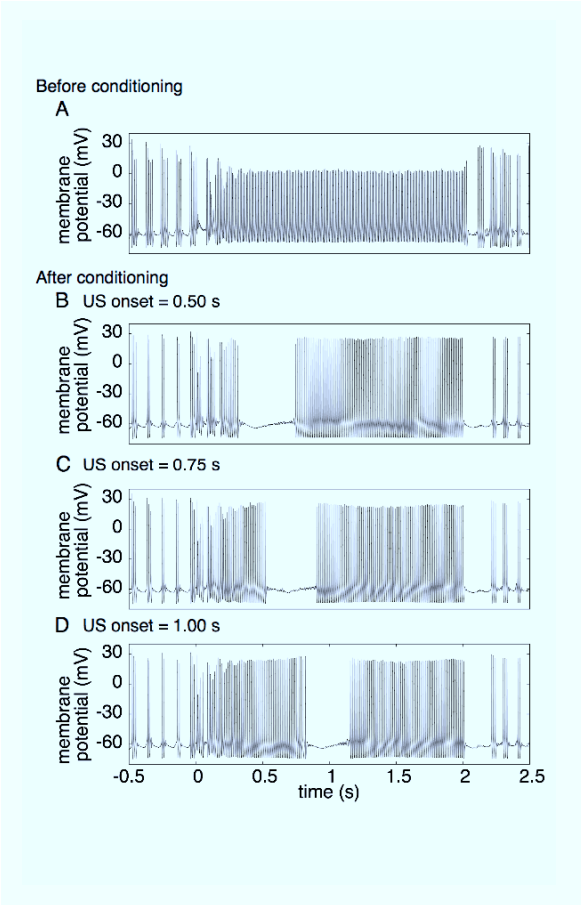

Figure 4.12: Membrane potential of a model PC in the simulation of delay eyeblink conditioning. A, Time evolution of membrane potential before conditioning. The abscissa indicates time from the CS onset. B, C and D, Time evolutions of membrane potential after conditioning in the cases where the US onset was set at 0.5, 0.75 and 1.0 s, respectively. The model PC learned to stop firing 100–200 ms earlier than the US onset for each conditioning.

Moreover, we conducted computer simulations using Equations 4.1 and 4.2. In this case, learning finished after several trials. We obtained qualitatively the same results about the cessation of the model PC firing from the LTD described by Equations 4.1 and 4.2 as the results from the simple LTD model (Figure 4.13). Furthermore, we obtained almost the same results from the LTD models using exponential functions instead of Gaussian functions for fitting to the two experimental data (data not shown). Therefore, we employed

the simple LTD model to avoid complexity unnecessary for the demonstration that POT representation in the granular layer network can be a basis for the induction of timed cessation of the PC firing.

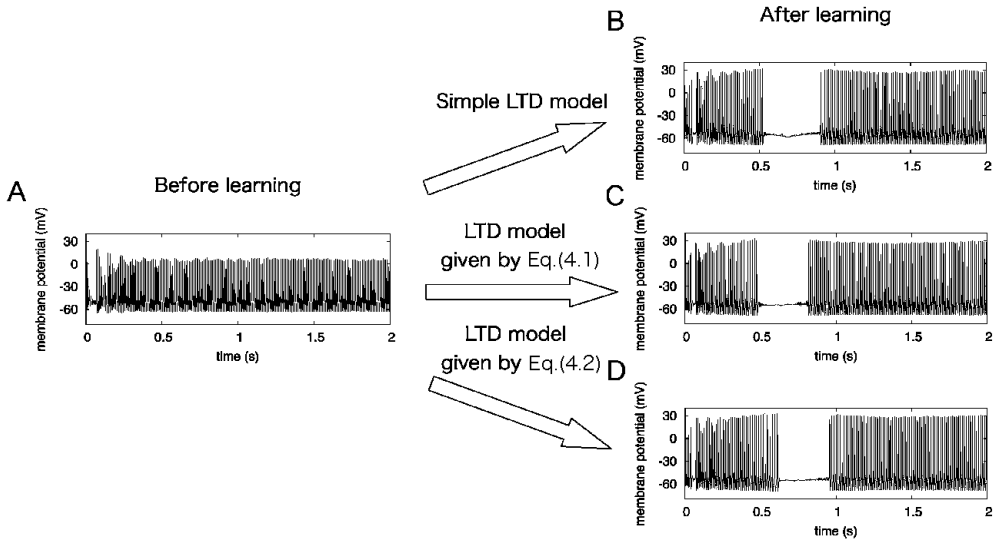

Figure 4.13: Model PC's membrane potentials in the simulations of delay eyelid conditioning. The left panel (A) shows membrane potential before conditioning, and three right panels represent membrane potentials after conditioning. The abscissa indicates time from the CS onset. The US onset was set at 0.75 s. B, C and D: the simple LTD model used in the present paper, LTD model given by Equation 4.1 and that given by Equation 4.2, respectively.

4.4 Discussion

4.4.1 Stimulus-dependent state transition of the model granular layer

In the present paper, we respectively modeled spontaneous MF activity and CS-evoked MF activity as small and large currents injected to grcs (Freeman and Muckler, 2003). The strength of the injected current controlled the network dynamics. Thereby, we demonstrated that an identical computational model of the cerebellar granular layer exhibited

both synchronized oscillation states (Maex and De Schutter, 1998) and POT-representing states (Yamazaki and Tanaka, 2007a; Medina et al., 2000; Buonomano and Mauk, 1994) depending on the strength of MF activity (Figure 4.14).

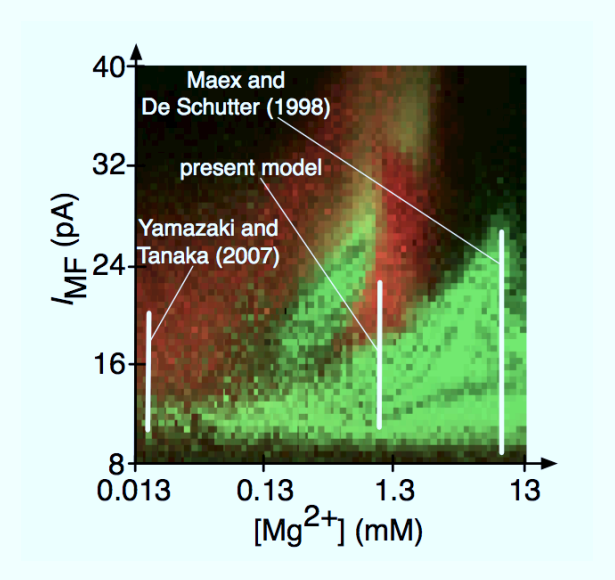

Figure 4.14: Parameter ranges mainly investigated in the present and previous research superimposed on the phase diagram.

When the network was driven by the low input current which represent spontaneous MF spikes, the model grcs and Gocs underwent the synchronized oscillation at 9 Hz, which may correspond to the oscillation of LFP found in animals staying at rest. This dynamics emerged from the mechanism proposed by Maex and De Schutter (1998). The oscillation frequency in our model was 9 Hz, whereas synchronized oscillation occurred at frequencies higher than 20 Hz in Maex and De Schutter's model. This discrepancy was due to the fact that we assumed a longer decay time constant of $GABA_AR$-mediated IPSPs at the model grcs. On the other hand, when a CS was fed to the network in our model, the model grcs exhibited random alternation between the burst firing and silent modes. Because the population of active grcs gradually changed with time without recurrence, we were able to conclude that there is a one-to-one correspondence between a certain population and a certain time from the CS onset. Therefore, the sequential activation of grc populations was able to represent the POT from the CS onset, as concluded by Yamazaki and Tanaka

(2007a).

The random alternation observed in the activities of model grcs emerged from the network dynamics, not from the noisy input stimuli. To verify this, we modeled MF signals as a deterministic current directly injected to model grcs instead of stochastic MF activities such as Poisson spikes.

We also conducted simulations of delay eyeblink conditioning to demonstrate that a model PC can read out a POT represented by the granular layer network. As a result of the simulated conditioning, the model PC learned to stop firing approximately 200 ms earlier than the US onset, which could trigger the cerebellar nucleus to develop the anticipatory CR.

4.4.2 Origin of random alternation between burst and silent modes

The present study has shown that a POT is represented by populations of active grcs, each of which exhibits random alternation of burst and silent modes. This raises a question of what the origin of the randomness in the mode alternation is. Maex and De Schutter (1998), in which synaptic weights of any connections in their network were random, did not show the random alternation of burst and silent modes of grcs. On the contrary, Yamazaki and Tanaka (2007a), in which the synaptic weights were constant though the connection pattern was random, demonstrated that the random alternation of the two modes emerged in grcs. These observations indicate that as long as synaptic connections between grcs and Gocs are random, fluctuation in synaptic weights of these connections is not important for the generation of the random alternation of the two modes. For the randomness in the external input, Medina et al. (2000) and Yamazaki and Tanaka (2007a) assumed that randomly generated spikes were fed to model grcs through MFs in order to demonstrate that a POT can be represented by populations of active grcs. However, the present model showed that the random alternation of burst and silent modes of grcs does not require noisy input to grcs. On the other hand, when we performed simulations using a modified model in which grcs and Gocs were all connected with each other so that the network did not have any randomness, activities of these cells exhibited only coherent oscillations. The above arguments indicate that the randomness in their connectivity is a major cause of

generating the random alternation between burst and silent modes in grcs and Gocs.

4.4.3 Influence of Golgi cells on the network dynamics

Buonomano and Mauk (1994) have shown that the precision of a timed CR elicitation became worse with increase in weights of MF synapses on Gocs, whereas activity patterns of grcs became more resistant to noise in MF input signals. In addition, Maex and De Schutter (1998) have observed that the synchronization of grc and Goc activities disappeared at stronger MF synapses on Gocs. These studies imply that the POT-representing states and synchronized oscillation states may disappear when we take into account direct MF inputs to Gocs, which are omitted in the present model. To examine the effects of the MF inputs to Gocs on the dynamical states, we performed additional simulations changing the ratio in strength of the current injected to Gocs to that injected to grcs, which would reflect the weight of MF synapses on Gocs relative to that on grcs, for two cases of a small and large currents injected to grcs. We found that OI was predominant over PI for any ratio of injected currents between 0 and 2 when the small current (10.7 pA) was injected to grcs, although both indices took small values when the ratio was large (Figure 4.15A). For the large current injection (22.7 pA), PI was larger than OI when the ratio of injected currents was smaller than 0.3, whereas OI was larger than PI when the ratio was between 0.3 and 1.3 (Figure 4.15B). The additional simulations by assuming a current injection to Gocs as well as grcs showed that there was a finite range of the strength of a current injected to Gocs, in which the POT-representing states or synchronized oscillation states appeared vigorously (Figures 4.15A and 4.15B). These results are consistent with Buonomano and Mauk (1994) for POT-representing states and Maex and De Schutter (1998) for synchronized oscillation states. Therefore, the dynamical features of the present model are validated for weak MF inputs to Gocs.

Recently, Dugué et al. (2009) have reported the existence of gap junctions between nearby Gocs and suggested that the oscillatory synchronization of Gocs can be induced from the electrical coupling. They also carried out computer simulation assuming the bath application of kainate to model Gocs and demonstrated that the Gocs mutually connected by gap junctions elicited spikes synchronously at 12 Hz. Their network model

was composed of model Gocs alone. It is unclear whether the Goc synchronization is preserved when connections with grcs that receive spontaneous spike input through MFs are taken into account.

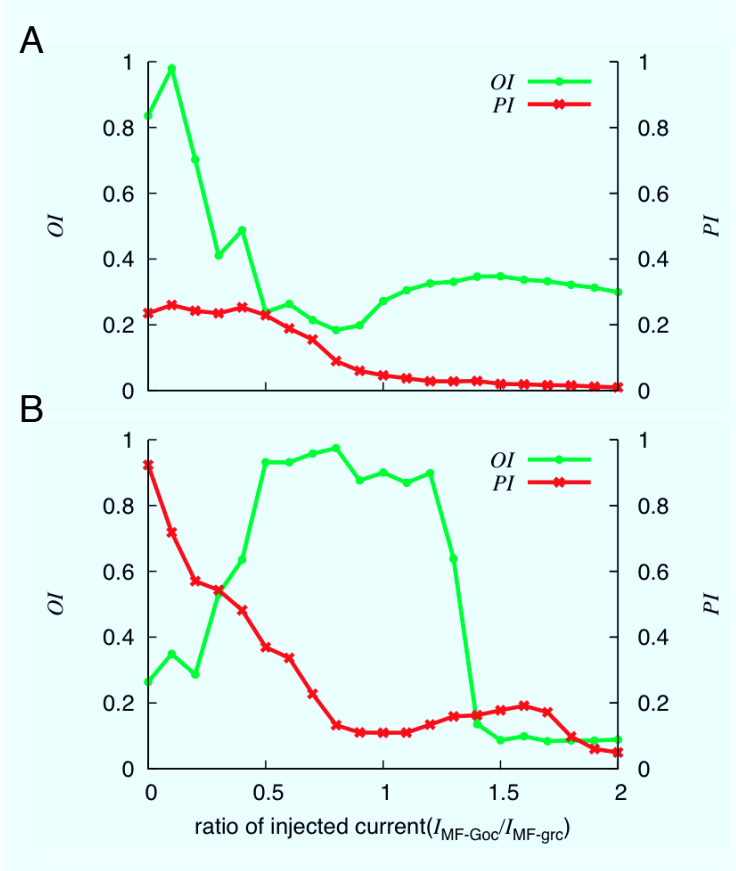

Figure 4.15: Oscillation index (OI) and POT-representation index (PI) for the injection of a small current ($I_{\text{MF-grc}} = 10.7$ pA in A) and a large current ($I_{\text{MF-grc}} = 22.7$ pA in B) while varying the ratio in strength of the current injected to Gocs to that injected to grcs. A, In the case of a small current injection to grcs, as the ratio increased, OI sharply decreased from nearly 1 to 0.3, whereas PI also decreased from 0.2 to nearly 0. B, In the case of a large current injection to grcs, as the ratio increased, OI showed a plateau between 0.5 and 1.2 of the ratio, whereas PI sharply decreased from 0.9 to 0.1.

4.4.4 Role of voltage dependence of NMDA channels in network-state transition

The key factor in the state transition between synchronized oscillation and POT representation was the voltage dependence of the simulated NMDA channels at model Goc dendrites. When the network was driven by simulated spontaneous MF spikes, the activity of model grcs was relatively low. Thus, the excitatory input signals to the model Gocs were weak. Thereby, model Gocs' activity was also relatively low, which did not effectively open the NMDA channels on the model Goc somas due to their voltage dependence. Thus, the model Gocs were mostly driven by AMPA channels, and hence the network behavior did not differ from that of Maex and De Schutter (1998)'s model. In contrast, when strong MF signals were fed to the network, the NMDA channels at the model Goc dendrites opened persistently because of vigorous excitatory input signals from the model grcs. This led to the alternation between the burst mode and the silent mode representing a POT, consistent with Yamazaki and Tanaka (2007a)'s model. The importance of the voltage dependence of the NMDA channels was confirmed by simulations under various concentrations of Mg^{2+}, which controls the opening of NMDA channels. We observed that the POT representation was disrupted by the blocking of NMDA channels, whereas the synchronized oscillation was disrupted by the persistent opening of NMDA channels at a low $[Mg^{2+}]$. Therefore, the NMDA channels are likely to be involved in the emergence of both the POT representation and the synchronized oscillation.

Even when we simply assumed the existence of NMDA channels at the Goc somas, the random alternation between the burst and silent modes was not found at model grcs in response to a CS. Rather, model grcs elicited single spikes regularly and intermittently instead of burst firing. This was because when a model Goc elicited a spike, the membrane potential quickly decreased to below the resting potential due to AHP, and the open NMDA channels closed immediately after the generation of a spike. Consequently, model Gocs did not elicit burst spikes. To open the NMDA channels for a longer time, NMDA channels should be located on the Goc dendrites, which are electrically isolated to some extent, as in the present model.

Furthermore, we varied the concentration of Mg^{2+} and the external input current to the

grcs to clarify the possible network states and the state transitions. For high [Mg^{2+}], which blocks synaptic transmission through NMDA channels, the POT representation in response to a CS was disrupted, and the grcs exhibited rapid oscillation with a small amplitude. With decreasing [Mg^{2+}], the amplitude of the rapid oscillatory activity increased (point 2). Then, the network entered a POT-representing state (point 3), a slow oscillation state (point 5) and finally a POT-representing state once again (point 6). On the other hand, synchronized oscillation during spontaneous MF activity was almost unaffected by changes in [Mg^{2+}]. With increasing the external input current, the network entered a rapid oscillation state (point 2), a POT-representing state (point 3) and finally a state with a high average firing rate (point 1).

Finally, we explored all possible dynamical states in the present network model by the varying values of [Mg^{2+}] and I_{MF} exhaustively. We determined the network dynamics of eight representative points and classified the eight points into four different states: a synchronized oscillation state (State I), a POT-representing state (State II), a metastable state (State III) and a uniform firing state (State IV). The present network model showed a rich variety of possible dynamic states.

4.4.5 Predictions based on the model

Gocs are regarded as playing an essential role in temporal information processing by the cerebellar cortex (D'Angelo, 2008). The present model specifically emphasizes the importance of voltage-dependent NMDA channels at Gocs. This leads to a prediction that blocking NMDA channels at Gocs disrupts POT representation and hence delay eyeblink conditioning. This prediction may be examined in the following way: NMDA channels at grcs consist of NR1, NR2A and NR2C subunits (Kadotani et al., 1996; Cull-Candy et al., 1998), whereas NMDA channels at Gocs consist of NR1, NR2B and NR2D subunits (Cull-Candy et al., 1998). Thus, NR2B subunits, which are selectively expressed at Gocs, can be responsible for the long-time opening of NMDA channels (Misra et al., 2000; Brickley et al., 2003), which is effective for the temporal integration of grc activities. Furthermore, NR2B subunits can be blocked selectively by ifenprodil (Misra et al., 2000; Brickley et al., 2003). Therefore, we may be able to observe the disruption of POT representation and

hence delay eyeblink conditioning by the application of ifenprodil.

Part II

Strength of a conditional stimulus

controls the timing of a conditional response

Chapter 5

Stimulus-strength-dependent timing control

5.1 Introduction

The cerebellum is widely accepted to control the performance of motor actions precisely (Ito, 1984). Achievement of temporally coordinated motor actions requires precise timing of each action. Very recently, we have proposed that neural dynamics of the granular layer in the cerebellar cortex represents the passage of time (POT) from the onset of a sustained CS conveyed by MFs as a temporal sequence of active grc populations (Yamazaki and Tanaka, 2005). Combining with LTD at synaptic junctions of PFs from grcs to PCs, which is induced by repetitive pairings with a CS and an US conveyed by the climbing fibers, PCs stop firing at the timing of the US presented during conditioning. The cessation of the PC firing releases tonic inhibition to cerebellar nucleus neurons that receive direct MF signals, and elicits a conditioned response (CR) as the nucleus neurons' activation. When we apply these computational mechanisms to the conditioning of motor reflex, it can be accounted for the temporal topography of a CR to a CS presentation. A typical example of such conditioning is Pavlovian delay eyeblink conditioning (for review, e.g., Mauk and Donegan, 1997; Hesslow and Yeo, 2002; Christian and Thompson, 2003). Particularly, in this conditioning, a subject is exposed to paired presentation of a sustained tone as a CS and an airpuff as a US that induces eyeblink reflex. After the repeated conditioning by

CS-US presentation with a fixed interstimulus interval (ISI) between the CS and US onsets, the CS presentation alone let the subject close the eye as a CR slightly prior to the US onset timing.

In our simulations of a conditioned cerebellar network, we found that spike trains elicited by grcs were extended or compressed for a CS stronger or weaker than the CS during the conditioning, which indicates that a stronger CS let a POT shorter whereas a weaker CS let it longer. This possibility is suggested by a recent experiment, in which a CR was elicited earlier when the strength of a tonal stimulus (CS) was increased. However, in the simulations, when we changed the strength of a CS, a model PC did not stop firing clearly. This suggests that the PC's read-out mechanism of a POT represented by grcs is not sufficient. In the present study, we incorporate a SC that inhibits the PC. We assumed that the model SC receives climbing fiber inputs and CS-US conjunctive stimulation induces long-term potentiation (LTP). Simulations showed that the model PC successfully stop firing earlier or later than the timing of a CR elicited by the CS presented during conditioning. It is suggested that SCs work to assist and enhance the PC's read-out mechanism of a POT.

5.2 Modeling of a CS

We model MF input signals as current injected directly to the model grcs, instead of spike trains. Freeman and Muckler (2003) have reported that the spontaneous firing rate of MFs is as low as 5 Hz, whereas the firing rate increases up to 30 Hz when stimulated with a tone (e.g. CS). We assume that the current into grcs increases with the frequency of firing conveyed through MFs. In simulations, we inject a current I_{MF} of 10.7 pA to all model grcs for 2 s to simulate grcs' activities induced by the spontaneous MF activity. For the succeeding 2 s, we inject a current I_{MF} of 29.5 pA to evoke grcs in response to high frequency MF firing induced by the presentation of the CS. Subsequently, we inject a current I_{MF} of 10.7 pA for 2 s again to resume the baseline activity of grcs induced by spontaneous MF activity. After conditioning, to simulate network dynamics under CSs of different strengths, we inject current of 31.0 pA or 28.5 pA into grcs.

5.3 Results

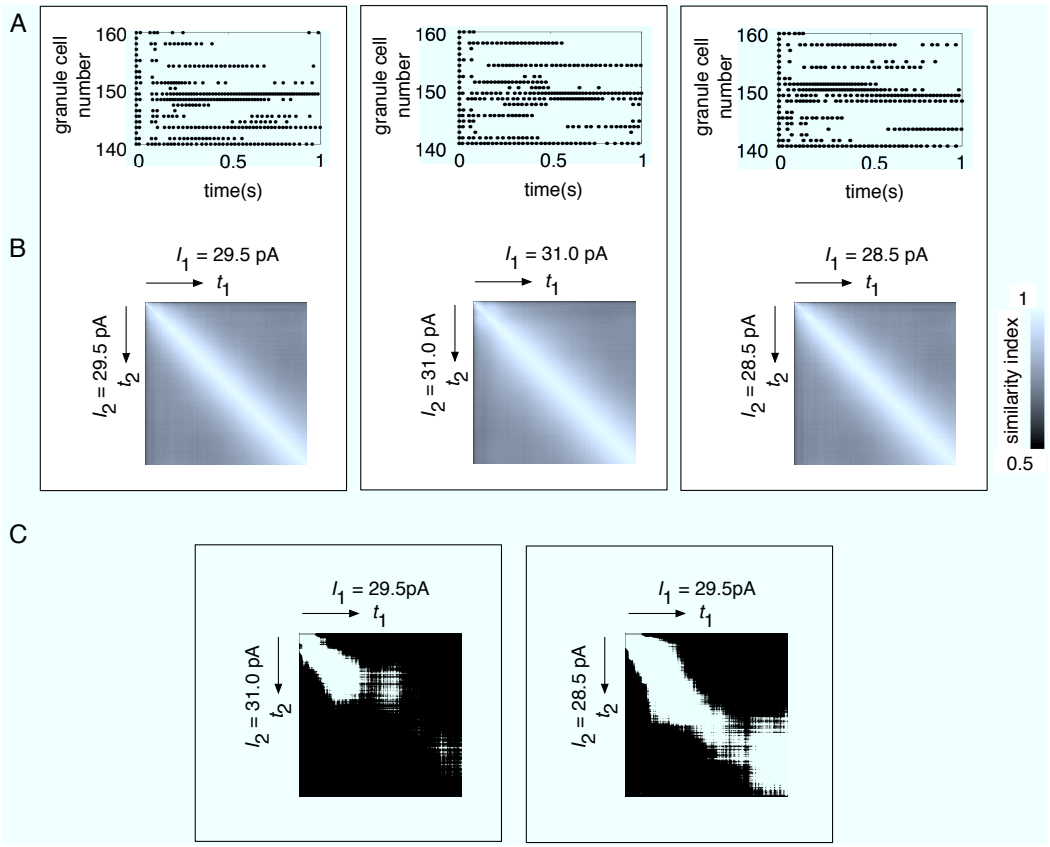

Figure 5.1: Network dynamics when current is injected to grcs as a CS input. (A) Spike patterns of 20 grcs. The abscissa and ordinate represent time and neuron index, respectively. (B) SI of spike patterns of grcs is plotted in a gray scale, in which black indicates 0.5 and white 1. (C) Network dynamics when currents of different strengths are injected to grcs. SI of spike patterns of grcs is plotted in a gray scale which black (white) indicates that SI is smaller (larger) than 0.80.

5.3.1 POT-representation

Figure 5.1A represents spike patterns of 20 model grcs in response to the sustained injection of current of 3 different strengths for simulated CSs. Activation of grcs by the CS presentation vigorously depolarizes randomly connected Gocs, resulting in the activation of voltage-gated NMDA channels on their dendrites. Because of the long decay time constant

of NMDAR-mediated EPSPs, Gocs inhibit nearby grcs, so that grcs exhibited random alternations between burst and silent states, as reported by Yamazaki and Tanaka (2007b) (See section 4.3.2). We show $SI(t_1, t_2)$ of spike patterns of grcs calculated with Equation 3 in a gray scale (Figure 5.1B) between 0.5 and 1. Even if the strength of injected current was different, larger $SI(t_1, t_2)$ appeared along the diagonal line and gradually decreased with the separation from the diagonal line. This shows that different grc populations were activated at different times, so that the population of active grcs changed gradually with time from the CS onset without recurrence. Therefore, the absence of recurrent populations of active grcs indicates one-to-one correspondence between a certain population of active grcs and a certain time, while the sustained current was injected as a CS signal. Thereby, the sequence of active grc populations is able to represent POT from the CS onset.

5.3.2 Speeding-up and slowing-down of an internal clock

Next, we compared a sequence of grc populations activated by the sustained injection of current of 29.5 pA with another sequence generated by the injection of current of 31.0pA (28.5 pA) using Equation 3.8. Figure 5.1C shows corresponding diagrams. The white band representing high similarity slanted slightly above (below) the diagonal line for the injection of stronger (weaker) current. This indicates that when strong (weak) current is injected, the sequence is compressed (extended). Namely, when input current is stronger (weaker), active grc populations appear earlier (later) and the speed of generation of active grc populations becomes faster (slower). The effect of the voltage-gated NMDA channels on the Goc dendrites in present model depends on the strength of a current injected to the network as we discussed above (See section 4.4.4). We hypothesis that the compressed (extended) sequence was generated by this effect. We show more results about this hypothesis in a next section.

5.3.3 Effect of voltage-gated NMDA channels on an internal clock

To examine whether the compressed (extended) sequence is generated by the voltage-gated NMDA channel on Goc dendrites, we performed a simulation under a nearly [Mg^{2+}]-free condition (0.013 mM). We also show $SI(t_1, t_2)$ of spike patterns of grcs calculated with

Equation 3.7 in a gray scale (Figures 5.2A, B and C) between 0.5 and 1. Even if the strength of injected current was different under this [Mg^{2+}] condition, larger $SI(t_1, t_2)$ appeared along the diagonal line and gradually decreased with the separation from the diagonal line. This result suggests that active grc population is able to represent POT form the CS onset even if [Mg^{2+}] is nearly free as we also indicated in part I. We also compared a sequence of grc populations activated by the sustained injection of current of 29.5 pA with another sequence generated by the injection of current of 31.0pA (28.5 pA). As shown in Figure 5.2D and E, larger $SI(t_1, t_2)$ appeared along the diagonal line. Namely, the two sequences were similar at a same time. This suggests that the speed of generation of active grc populations is independent on the strength of an injected current when [Mg^{2+}] is nearly free. Thereby, it is indicated that the speed is changed by the effect of the voltage-gated NMDA channels on the Goc dendrites.

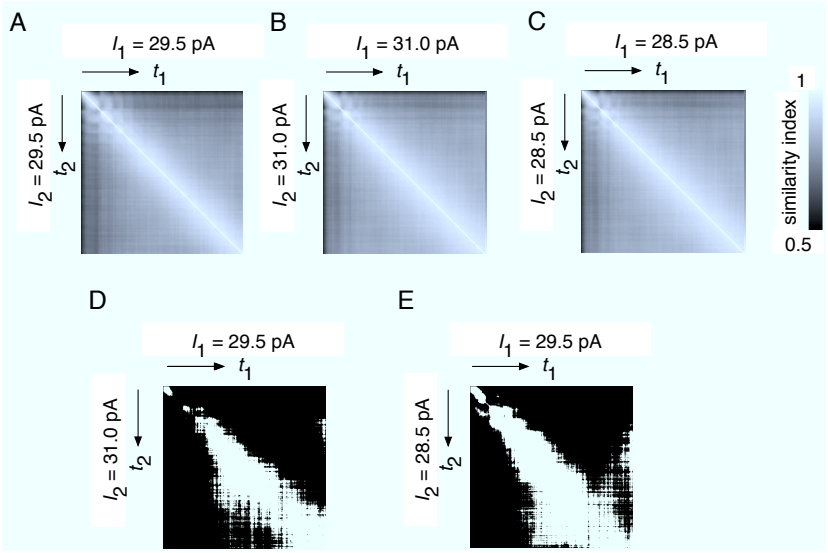

Figure 5.2: Network dynamics when NMDA channels on Gocs open continuously. (A) and (B) SI of spike patterns of grcs to which we injected a current I_{MF} of 29.5 pA (A) and 31.0 pA(B) is plotted in a gray scale, in which black indicates 0.5 and white 1. (C) Network dynamics when currents of different strengths are injected to grcs. SI of spike patterns of grcs is plotted in a gray scale which black (white) indicates that SI is smaller (larger) than 0.85.

5.4 Simulation of delay eyeblink conditioning

5.4.1 Cerebellar model

The model network contains 1 PC and 1 SC (Figure 5.4). The model PC and SC receive PF inputs from grcs and climbing fiber inputs that convey US signals. The SC sends an inhibitory connection to the PC.

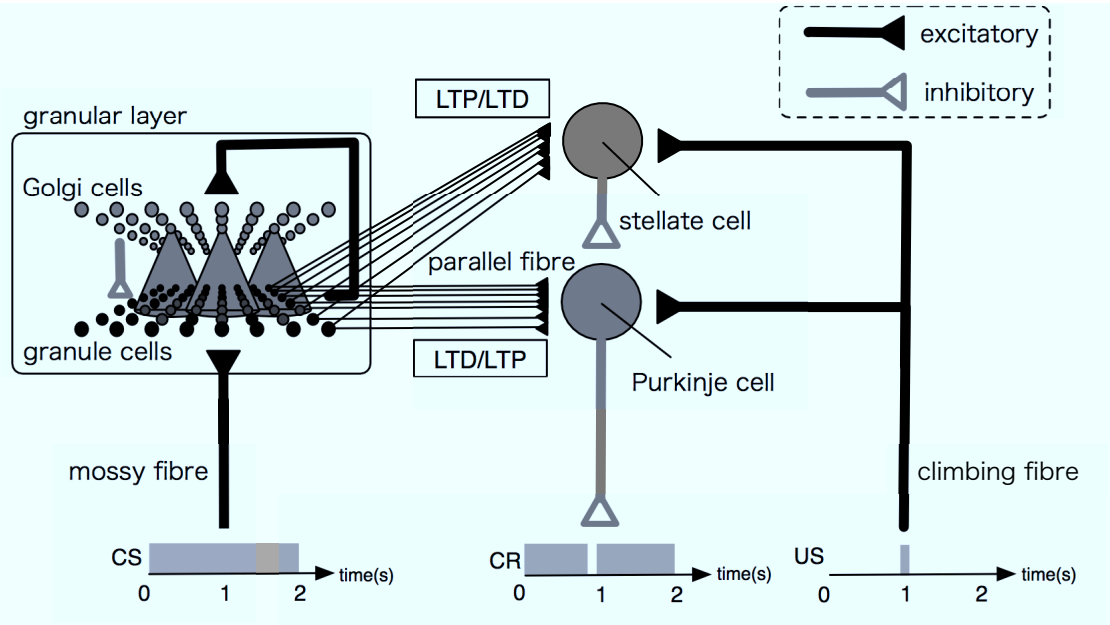

Figure 5.3: A schematic of the cerebellar network model. Gocs receive excitatory inputs from grcs and recurrently inhibit grcs. Thus, grcs and Gocs construct a recurrent inhibitory network. Grcs receive CS signals and, in turn, excite a PC and SC. Paring of US signals fed to a PC and SC with CS signals induce LTD and LTP at parallel fiber terminals at these cells.

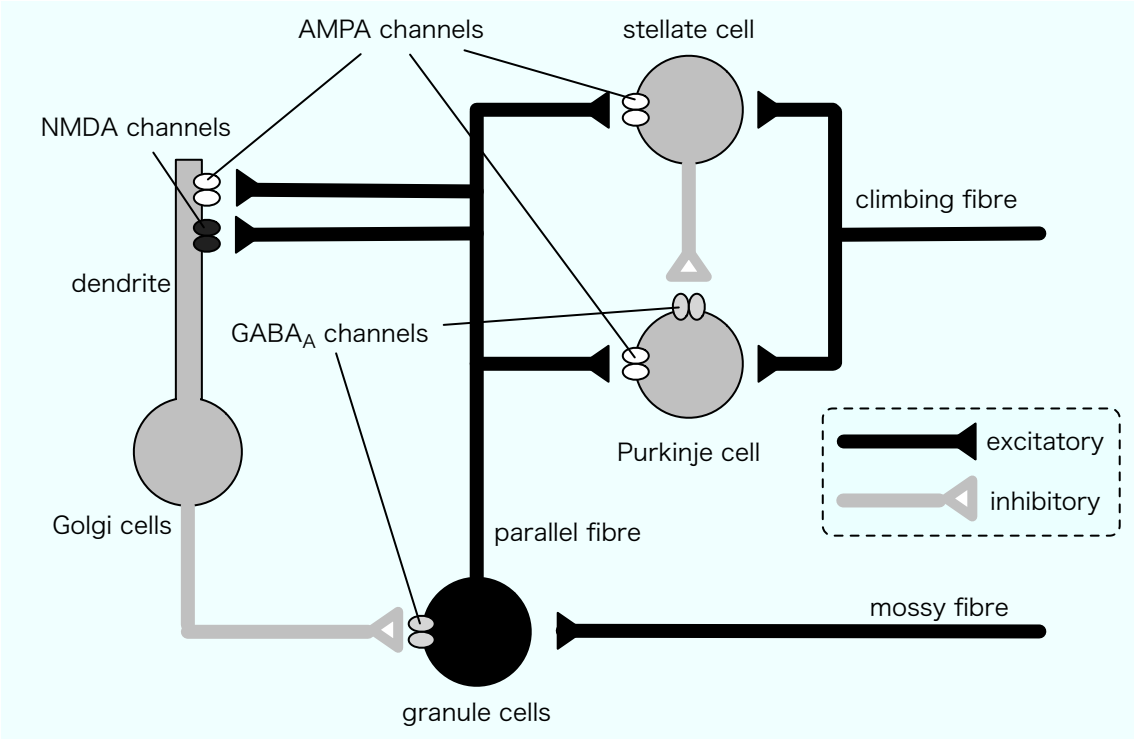

Figure 5.4: Grcs' excitation of Gocs is mediated by AMPA and NMDA channels, whereas Gocs' inhibition of grcs is mediated by $GABA_A$ channels. The strength of current into grcs, which is induced by mossy fiber signal, is external stimulus strength as a control parameter in this model. A PC and a SC are excited by the grcs mediated by AMPA channels. The PC is inhibited by the SC mediated by $GABA_A$ channels.

Purkinje and stellate cell models

A PC and an SC are modeled as single-compartment Hodgkin-Huxley units. These cells are assumed to be excited by PF inputs from grcs mediated by the activation of AMPA channels. The PC is assumed to be inhibited by the SC through $GABA_A$ channels.

Plasticity of PF synapses of a Purkinje and stellate cell

For eyeblink conditioning, we present US signal 650 ms after the onset of CS signal presentation. The US signal is sent to both PC and SC. Before conditioning, we set synaptic weights of all PFs at $w_i^{(0)} = 1$ and $v_i^{(0)} = 1$ for the PC and the SC, respectively. During

conditioning, conjunctive stimulation of a CS and a US is assumed to induce LTD and LTP at PF synapses to the PC and the SC, respectively. According to Equations 5.1 and 5.2, these synaptic weights are decreased at the PC and increased at the SC when the PFs are activated 50-100 ms before the onset of a US. In addition, we also assume that when spike activity is transmitted to the PC and the SC through PFs alone, PF synapses undergo LTP and LTD, respectively.

$$w_i^{(T_r)} = w_i^{(Tr-1)} 0.9^f 1.0005^{f_{total}-f}. \tag{5.1}$$

$$v_i^{(T_r)} = v_i^{(Tr-1)} 1.07^f 0.985^{f_{total}-f}. \tag{5.2}$$

Here, f is the frequency of firing of ith grc in the interval of 50-100 ms immediately before the onset of a US. f_{tatal} is the total frequency of firing during one trial of conditioning for 2 s. T_r is the trial number. For simplicity, we assume that the US through the climbing fibers affects only learning of PF synaptic weights but not the neurons' activity.

Simulation of delay eyeblink conditioning

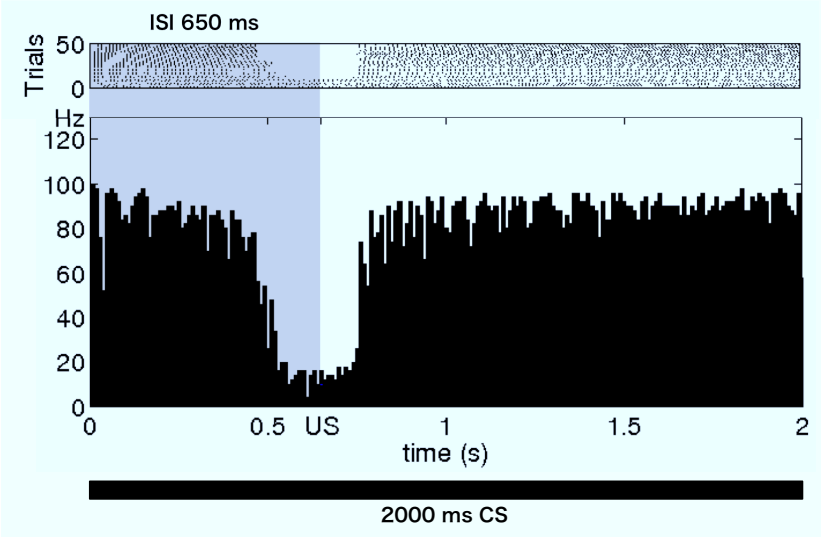

Figure 5.5: A Purkinje cell CR pause that was preceded and followed by an excitatory response. Upper panel shows raster plot of active Purkinje cell. Bottom panel indicate histogram of responses from a cell conditioned to the 650 ms CS-US interval, using a CS of 2000 ms duration. A Purkinje cell CR pause that was preceded and followed by an excitatory response. The abscissa represents time from the onset current of current injection.

Cerebellum model of delay eyeblink conditioning

We conducted simulations of delay eyeblink conditioning, in which current injection representing a CS generates a non-recurrent sequence of active grc populations and a US presented after the CS onset changes synaptic weights of PFs from model grcs to the model PC and the SC inhibiting the PC. Before conditioning, the model PC fired at high frequency during the CS presentation (injected current: 29.5 pA). In conditioning, a US signal was given 650 ms after the CS onset. For the model PC, LTD was induced at PF synapses connecting from grcs active at the timing of the US presentation. For the SC, LTP was induced at PF synapses from those active grcs. During paired CS-US presentation, PC firing stop which elicit the CR gradually appeared in response to the CS that decreased simple spike activity of a PC (Figure 5.5), supported by experiment results (Jirenhed and

Hesslow, 2011). After 50 trials of conditioning, when we injected current of the same strength as in the conditioning as a CS signal, the PC began to stop firing between 516 ms and 754 ms from the CS onset (Figure 5.6A). This result indicates that the model PC was able to learn an ISI between CS and US onsets, as consistent with an experiment (Jirenhed et al., 2007). On the other hand, when we injected current of 31.0 pA (28.5 pA) as a strong (weak) CS signal, the PC began to stop firing 161ms earlier (898 ms later) than in the default (Figure 5.6B and C). These observations indicate that after conditioning, when a stronger (weaker) CS signal is presented than a CS signal used in conditioning, a PC stopped firing earlier (later). This suggests that even after conditioning, the timing when a CR is elicited can be controlled by the strength of a CS signal.

Effect of molecular interneurons on delay eyeblink conditioning

Next, we examined how the model SC is involved in this timing control after conditioning, by removing the SC after conditioning. First, we injected current of 29.5 pA, the PC began to stop firing between 541 ms and 652 ms after the CS onset (Figure 5.6D). Although the duration of the PC firing cessation was shorter than that in the default case, the qualitative features of the firing was preserved without the SC. However, when we injected current of 31.0 pA or 28.5 pA after conditioning, the PC kept tonic firing, indicating that the ISI coding was disrupted (Figure 5.6E, F). This suggests that the SC plays an important role for adaptive timing control. Also, when we blocked the plasticity of PF synapses at the SC during conditioning, the PC behaved similarly to the case which a model SC was removed (data not shown).

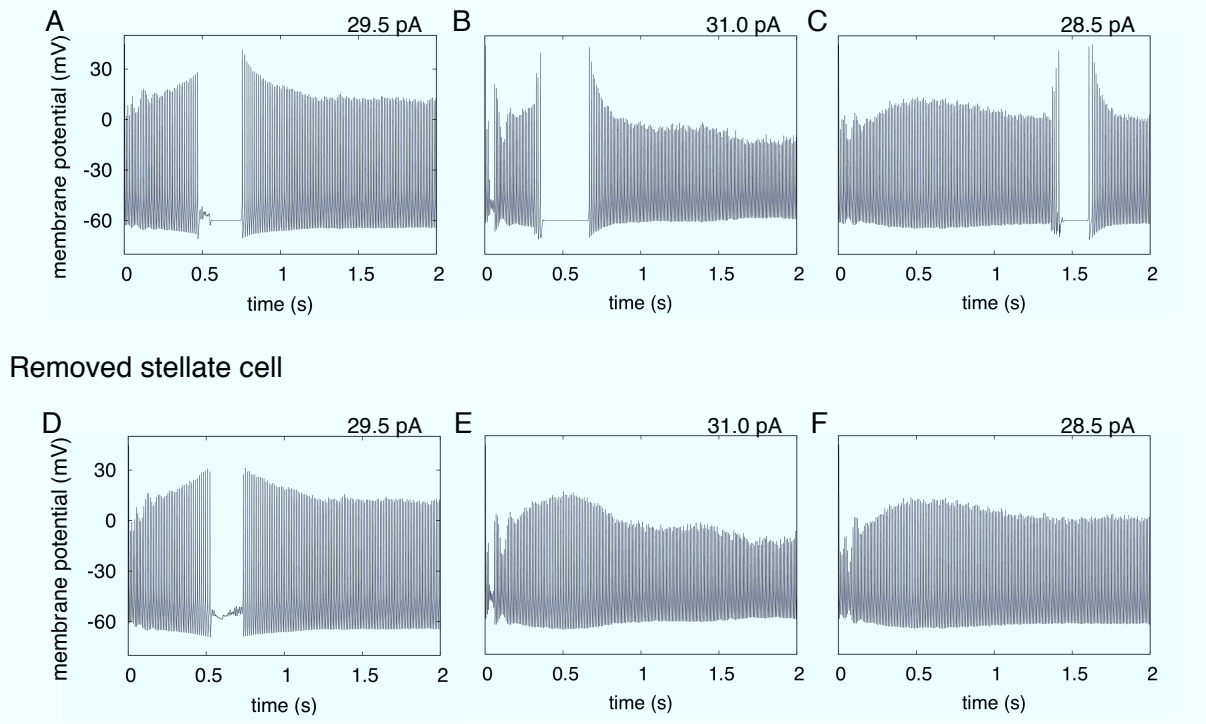

Figure 5.6: Membrane potential of a PC in the simulation of eyeblink conditioning. In conditioning, US signal is fed to the PC at 650 ms after sustained injection of current of 29.5 pA to grcs. (A) Membrane potential in response to sustained current of 29.5 pA to grcs after conditioning and (D) membrane potential after SC was removed. (B) Membrane potential in response to sustained injection of current of 31.0 pA and (E) membrane potential after SC was removed. (C) Membrane potential in response to sustained injection of current of 28.5 pA and (F) membrane potential after SC was removed. The abscissa represents time from the onset of current injection, and the ordinate represents membrane potential.

Effect of LTD on synapses between parallel fibers and Purkinje cell

Which is main pathway in the cerebellum when an animal learns to a appropriate timing, MF-grc-SC-PC or MF-grc-PC pathway (Svensson et al., 2010) In order to confirm even if MF-grc-PC pathway is more important than another pathway, we blocked the plasticity of PF synapses at the PC during conditioning. When only CS (injection of current of 29.5 pA) was presented after this conditioning, the PC maintained tonic firing (Figure 5.7A). Thus, the PC did not memorize the appropriate timing of US. As shown Figures 5.7B

and C, the PC did not pause even if the strength of the injected current was changed. These results indicate that (1) PC can memorize an appropriate timing on the MF-grc-PC pathway and (2) PC can read out a certain pattern from compressed (extended) sequence on the MF-grc-SC-PC pathway.

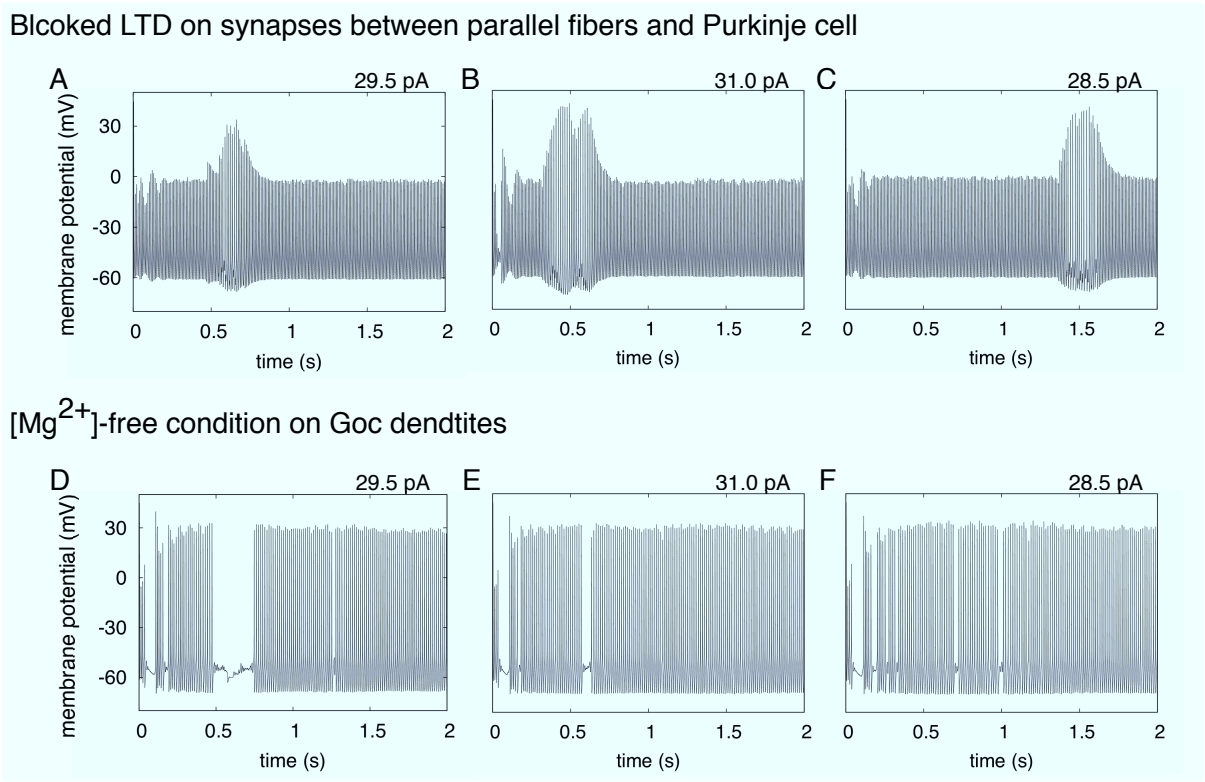

Figure 5.7: Membrane potential of a PC in the simulation of eyeblink conditioning. In conditioning, US signal is fed to the PC at 650 ms after sustained injection of current of 29.5 pA to grcs. (A) Membrane potential in response to sustained current of 29.5 pA to grcs after conditioning when LTD on synapses between PF and a PC was blocked before conditioning and (D) membrane potential under $[Mg^{2+}]$-free condition. (B) Membrane potential in response to sustained injection of current of 31.0 pA when the LTD was blocked and (E) membrane potential under $[Mg^{2+}]$-free condition. (C) Membrane potential in response to sustained injection of current of 28.5 pA when the LTD was blocked and (F) membrane potential under $[Mg^{2+}]$-free condition. The abscissa represents time from the onset of current injection, and the ordinate represents membrane potential.

Effect of voltage-dependent NMDA channels on Golgi cell dendrites

We confirmed that compressed (extended) sequence was generated by an effect of voltage-dependence of NMDA channels on Goc dendrites (see section 5.3.3). Next, we explored PC activities under [Mg^{2+}]-free condition. When we injected current of the same strength as in the conditioning as only CS was presented (injection of current of 29.5 pA) after 71 trials of conditioning, the PC began to stop firing between 473 ms and 747 ms from the CS onset (Figure 5.7D). This suggests that PC was able to learn an ISI between CS and US onsets when [Mg^{2+}] is nearly free in the POT-presenting state. Moreover, when only stronger (weaker) CS was presented (injection of current of 31.0 pA (28.5 pA)) after this conditioning, the PC stopped firing in shorter term (567–634 ms (688–724 ms)) (Figure 5.7E (F)). Becase the sequence was not compressed due to [Mg^{2+}]-free condition, the timing of firing stop of PC was not earlier. These indicates that voltage-dependence of the NMDA channels is one of the important factors of changing CR timing.

5.5 Discussion and conclusion

Adaptive control of timing by the strength of external stimulus seems essential for the generalization of motor actions. For example, in batting, we swing a bat at an appropriate timing to hit the ball, estimating the speed of a pitched ball visually. If the speed of a pitched ball is high, we start swinging the bat faster unconsciously. It is expected that the cerebellum learns the timing of motor actions in a supervised manner and controls the learned timing adaptively (Ivry, 1996). In the present study, using our spiking network model of the cerebellar cortex, we argued that a stronger or weaker CS signal conveyed by MFs makes the POT representation change by compressing or expanding the temporal sequence of active grc populations. Learned timing was advanced or delayed as shown by the temporal shift of timed pause of the PC in the simulated Pavlovian delay eyeblink conditioning, as consistent with experimental findings (Svensson et al., 2000). Our results indicate that the cerebellar cortex controls a timing rather than the cerebellar nuclei, supported by Svensson et al. (2010).

5.5.1 Role of stellate cells in cerebellar adaptive timing control

We are particularly interested in the role of SCs in the adaptive control of the learned timing. We demonstrated that removing the model SC from the network disrupts the expression of the timing, suggesting that SCs assist the coding of a timing by PCs in motor control, as hypothesized by Rancillac and Cr??pel (2004). To date, little attention has been paid to the functional role of SCs, except a classical hypothesis as a gain controller of PCs to keep the activity level of PCs within a physiological range by inhibiting them in a feed-forward manner (Marr, 1969; Albus, 1971). The present study shed light for the first time on the functional role of SCs in cerebellar adaptive timing control.

5.5.2 Role of voltage dependence NMDA channels on Golgi cell dendrite in cerebellar adaptive timing control

It was possible to speed up/slow down the sequence generation as the strength of input stimuli increases/decreases. This is because a time constant of NMDA channels on Gocs was changed with strength of MF input stimuli as a CS signal by the voltage-dependence of NMDA channels. When the concentration of Mg^{2+} was low; NMDA channels continually opened, it was impossible to change the clock speed. Furthermore, in this condition, a PC stop firing at US timing when the strength of input stimuli after conditioning. This suggested that NMDA channels on Goc dendrites are necessary for the temporal shift of timed pause of the PC.

5.5.3 Cerebellar cortex as a liquid state machine

The cerebellum is regarded as a universal simulator that simulates the dynamics of physical and mental objects by acquring the internal models through supervised learning (Daniel et al., 1998; Ito, 2008). The present network model of the cerebellar cortex consists of the granular layer that generates a temporal sequence of active grc populations as liquid states, and a unit composed of a PC and an SC that receives the sequence and extracts time-varying information from the sequence. Once we interpret the granular layer and a PC-SC unit respectively as a reservoir and a readout, our model turns out to be equivalent to a liquid state machine (LSM) (Yamazaki and Tanaka, 2007b), a type of artificial

neural network model, which is a universal supervised learning machine (Maass et al., 2002). In conventional LSMs, a readout is simply a single model neuron that recruits a simple perceptron learning scheme. In contrast, the readout in our model is a pair of two neurons recruiting plasticity of the opposite direction. By this combination, the model cerebellar cortex is able to generalize the timing of a CR adaptively by the strength of a CS signal. This suggests the enhancement of the ability of reading out information from the liquid state in the granular layer. Therefore, the present study may provide insight into the computational power of the cerebellum as a biological counterpart of a liquid state machine. This study also suggests that LSMs can be improved by incorporating inhibitory interneurons in the readout unit.

Chapter 6

Summary

Information processing of the cerebellar granular layer composed of grcs and Gocs is regarded as an important first step toward the cerebellar computation.

Intensive studies of Pavlovian delay eyeblink conditioning have suggested that the cerebellum can memorize a POT from the onset of an external stimulus. To account for possible mechanisms of such POT representation, some network models have been proposed to show that grcs in the cerebellar granular layer can exhibit random alternation of burst and silent modes under feedback inhibition from Gocs, resulting in non-recurrent generation of active grcs populations. On the other hand, the oscillation of LFP has been observed in the cerebellar granular layer when animals stay at rest. Some network models have shown that grcs can elicit synchronous spikes in an oscillatory manner. These qualitatively different neural dynamics of the granular layer raises a question of how they can be accounted for by an identical network in the cerebellar granular layer. Here we report that grcs activities of a biologically plausible spiking network model undergo the transition between synchronized oscillation and random alternation of burst and silent modes, depending on the strength of MF input (Figure 4.14). We found that the voltage dependence of N-methyl-D-aspartate (NMDA) channels assumed at dendrites of model Gocs acts as a switch between the two modes of neural dynamics. We also found that grc activity pattern which represent the POT, compressed (extended) due to the effect of NMDA channels on Goc dendrites when strong (weak) input current is injected to grcs. This suggests that the speed of an internal clock depends on the strength of the injected current. Thus, our network model of the

cerebellar granular layer show a more variable dynamics depending on the strength of MF input than a liquid state generator in a LSM (Yamazaki and Tanaka, 2007b).

We performed simulations of delay eyeblink conditioning in the representation of POT between onsets of conditioned and unconditioned stimuli. We added a model PC and inhibitory cell (SC or BC) to the present model and simulated LTD and LTP at PF-PC synapses and PF-inhibitory cell synapses. We observed that the PC successfully learned to stop firing at the onset of the unconditioned stimulus and the timing of the stop changed by the strength of MF input. This suggests that the timing of the condition response is controlled by the strength of MF input in delay eyeblink conditioning. When the strength was changed after conditioning and removing a inhibitory internal cell, the PC kept tonic firing. When plasticity of PF synapses at the PC was blocked, the PC maintained tonic firing. This indicates that an internal cell (SC or BC) help the PC to read out more information than read out neurons model in a LSM (Yamazaki and Tanaka, 2007b). Thus, our model predicts that the cerebellar cortex has more computational power of the entire network than a LSM. In next study, we have to definitely show how computational power our network model has.

While a MF input is converted to a nuclear output through a microcomplex, the input–output relationship is modifiable due to LTD induced in the microzone by teaching signals conveyed by the climbing fibers. A microcomplex is an adaptive unit of the cerebellum; like a computer chip, it is attached to a bodily control system, affording it with adaptiveness (Ito, 1984). Based on this Ito's idea (Ito, 1984), we reproduced a cerebellar function as a liquid state machine on a FPGA (Field programable gate array) (Matsuno et al., 2010), which we called for a cerebellar computer chip. In the future, we can add our findings introduced in the present thesis to our cerebellar computer chips, which may be applied to robot control system of artificial muscle actuators.

Appendix

Neuron Model	
Name	Granule cell (grc)
Type	Hodgkin-Huxley
Dynamics	$I_{\text{applied}} = C\frac{dV}{dt} + \frac{1}{R}(V - V_{\text{leak}}) + \sum_{\text{channel}} g_{\text{channel}}(V - V_{\text{channel}})$ $+ \sum_{\text{synapse}} g_{\text{synapse}}(V - V_{\text{synapse}}) + I_{\text{input}}$ with $C = 3.14\text{pF}, R = 9.65\text{G}\Omega, -70\text{mV} < V_{\text{leak}} < -60\text{mV}$
Voltage-gated channels	$g_{\text{channel}}(t,V) = \bar{g}m^P h$ $\frac{dm}{dt} = \alpha(1-m) - \beta m, \quad \tau = \frac{1}{\alpha+\beta}, \quad m_\infty = \frac{\alpha}{\tau}$ Exponential(Exp): $\alpha(V) = Ae^{B(V_m - V_0)} + C$ Sigmoid(Sig): $\alpha(V) = \frac{A}{1+e^{B(V_m - V_0)}}$ Linoid(Lin): $\alpha(V) = \frac{A(V_m - V_0)}{e^{B(V_m - V_0)} - 1}$ KC α: $\alpha(V,[\text{Ca}^{2+}]_i) = \frac{A}{1+\frac{Ce^{BV_m}}{[\text{Ca}^{2+}]_i}}$ KC β: $\alpha(V,[\text{Ca}^{2+}]_i) = \frac{A}{1+\frac{[\text{Ca}^{2+}]_i}{Ce^{BV_m}}}$
$GABA_A$	$g_{\text{synapse}}(t,V) = \bar{g}\frac{(\tau_1 - \tau_2)(e^{-\frac{t}{\tau_1}} - e^{-\frac{t}{\tau_2}})}{\tau_1\tau_2(e^{-\frac{t_{\text{peak}}}{\tau_1}} - e^{-\frac{t_{\text{peak}}}{\tau_2}})}$ with $t_{\text{peak}} = \frac{\tau_1\tau_2\ln(\frac{\tau_1}{\tau_2})}{\tau_1 - \tau_2}, t_1 = 100\text{ms}, t_2 = 5\text{ms}, \bar{g} = 314\text{pS},$ $V_{\text{synapse}} = -70\text{mV}$

Calcium pools	$\frac{d[\mathrm{Ca}^{2+}]_i}{dt} = \frac{I_{\mathrm{CaL}}}{2FAd} - \frac{[\mathrm{Ca}^{2+}]_i - [\mathrm{Ca}^{2+}]_{\mathrm{rest}}}{\tau}$ with $[\mathrm{Ca}^{2+}]_{\mathrm{rest}} = 75.5\mathrm{nM}$, F = 96,494C/mol, $\tau = 10\mathrm{ms}$, A = $314\mu\mathrm{m}^2$, $d = 0.084\mu\mathrm{m}$
Mossy fiber input	We regarded mossy fiber input as current injected to all grcs.
Golgi cell input	Each model grc randomly receives connections from Gocs within grc dendritic arborization diameter 315μm (the mean and standard deviation of the connection is 6.11 and 2.57) (Fig.1).

Neuron Model	
Name	Golgi cell (Goc)
Type	Hodgkin-Huxley
Dynamics	$I_{\mathrm{applied}} = C\frac{dV}{dt} + \frac{1}{R}(V - V_{\mathrm{leak}}) + \sum_{\mathrm{channel}} g_{\mathrm{channel}}(V - V_{\mathrm{channel}})$ $+ \frac{V' - V}{R_{\mathrm{a}}} + C'\frac{dV'}{dt} + \frac{1}{R'}(V' - V'_{\mathrm{leak}}) + \sum_{\mathrm{synapse}} g_{\mathrm{synapse}}(V - V_{\mathrm{synapse}})$ with $C = 28\mathrm{pF}$, $R = 10.7\mathrm{G\Omega}$, $C' = 18.9\mathrm{pF}$, $R' = 1.6\mathrm{G\Omega}$, $R_{\mathrm{a}} = 3.82\mathrm{M\Omega}$, $-60\mathrm{mV} < V_{\mathrm{leak}} < -50\mathrm{mV}$
Voltage-gated channels	$g_{\mathrm{channel}}(t,V) = \bar{g}m^P h$ $\frac{dm}{dt} = \alpha(1-m) - \beta m, \quad \tau = \frac{1}{\alpha+\beta}, \quad m_\infty = \frac{\alpha}{\tau}$ Exponential(Exp): $\alpha(V) = Ae^{B(V_m - V_0)} + C$ Sigmoid(Sig): $\alpha(V) = \frac{A}{1 + e^{B(V_m - V_0)}}$ Linoid(Lin): $\alpha(V) = \frac{A(V_m - V_0)}{e^{B(V_m - V_0)} - 1}$ KC α: $\alpha(V,[\mathrm{Ca}^{2+}]_i) = \frac{A}{1 + \frac{Ce^{BV_m}}{[\mathrm{Ca}^{2+}]_i}}$ KC β: $\alpha(V,[\mathrm{Ca}^{2+}]_i) = \frac{A}{1 + \frac{[\mathrm{Ca}^{2+}]_i}{Ce^{BV_m}}}$

AMPA	$g_{\text{synapse}}(t,V) = \bar{g}\dfrac{(\tau_1-\tau_2)(e^{-\frac{t}{\tau_1}}-e^{-\frac{t}{\tau_2}})}{\tau_1\tau_2(e^{-\frac{t_{\text{peak}}}{\tau_1}}-e^{-\frac{t_{\text{peak}}}{\tau_2}})}$ with $t_{\text{peak}} = \dfrac{\tau_1\tau_2\ln(\frac{\tau_1}{\tau_2})}{\tau_1-\tau_2}$, $t_1 = 0.5\text{ms}$, $t_2 = 0.03\text{ms}$, $\bar{g} = 23{,}500\text{pS}$, $V_{\text{synapse}} = 0\text{mV}$
NMDA	$g_{\text{synapse}}(t,V) = \bar{g}\dfrac{(\tau_1-\tau_2)(e^{-\frac{t}{\tau_1}}-e^{-\frac{t}{\tau_2}})}{\tau_1\tau_2(e^{-\frac{t_{\text{peak}}}{\tau_1}}-e^{-\frac{t_{\text{peak}}}{\tau_2}})(1+\eta[\text{Mg}^{2+}]e^{-\gamma V_m})}$ with $t_{\text{peak}} = \dfrac{\tau_1\tau_2\ln(\frac{\tau_1}{\tau_2})}{\tau_1-\tau_2}$, $t_1 = 100$, $t_2 = 5$, $\bar{g} = 2{,}520\text{pS}$, $V_{\text{synapse}} = 0\text{mV}$, $\eta = 0.00092\text{mM}^{-1}$, $\gamma = 150\text{mV}^{-1}$, $[\text{Mg}^{2+}] = 1.2\text{mM}$
Calcium pools	$\dfrac{d[\text{Ca}^{2+}]_i}{dt} = \dfrac{I_{\text{CaL}}}{2FAd} - \dfrac{[\text{Ca}^{2+}]_i - [\text{Ca}^{2+}]_{\text{rest}}}{\tau}$ with $[\text{Ca}^{2+}]_{\text{rest}} = 75.5\text{nM}$, F = 96,494C/mol, $\tau = 200\text{ms}$, A = 2,826μm^2, $d = 0.091\mu\text{m}$
granule cell input	Each model Goc randomly connected from closed 9×32 PFs (the mean and standard deviation of the connection is 26.80 and 6.50) (Fig.1).

Parameter values of voltage-gated channels for model grc and Goc											
Channel	$V_{channel}$ (mV)	P				A (ms^{-1})	B (ms^{-1})	C (ms^{-1})	V_0 (mV)	Constraints	$\bar{g}$ (nS)
NaF	55	3	m	α	Exp	7.5	0.081		-39		grc
				β	Exp	7.5	-0.066		-39	$\tau > 0.01$ ms	172
			h	α	Exp	0.6	-0.089		-50		Goc
				β	Exp	0.6	0.089		-50	$\tau > 0.045$ ms	1,131
Kdr	-90	4	m	α	Exp	0.85	0.073		-38		grc
				β	Exp	0.85	-0.018		-38		28
			h	α	Exp	3e-4	-0.08	35e-4	-46	$\alpha > 38e-4$	Goc
				β	Sig	5.5e-3	-0.0807		-44		192
CaL	80	2	m	α	Sig	8.0	-0.072		5		grc
				β	Lin	0.1	0.2		-8.9		2.9
			h	α	Exp	0.025	-0.05		-60	$\alpha > 0.025$	Goc
				β	Exp	-0.025	-0.05	0.025	-60	$\beta > 0.0$	23.5
H	-42	1	m	α	Exp	4e-3	-0.0909		-75		grc 97.1
				β	Exp	4e-3	0.0909		-75		Goc 4.85
KA	-90	3	m	τ	Exp	0.41	1/42.8	0.167	-43.5		grc
				m_∞	Sig	1	-1/19.8		-46.7		3.6
			h	τ	$\tau(V) = 10.8 + 0.03V_m + 1/(57.9e^{0.127V_m} + 0.000134e^{-0.059V_m})$						Goc
				h_∞	Sig	1	1/8.4		-78.8		14.8
KC	-90	1	m	α	KCα	12.5	-0.085	1.5e-3			grc 56.5
				β	KCβ	7.5	-0.077	150e-6			Goc 16.2

Neuron Model	
Name	Purkinje cell (PC)
Type	Hodgkin-Huxley
Dynamics	$I_{\text{applied}} = C\frac{dV}{dt} + \frac{1}{R}(V - V_{\text{leak}}) + \sum_{\text{channel}} g_{\text{channel}}(V - V_{\text{channel}}) + \sum_{\text{synapse}} g_{\text{synapse}}(V - V_{\text{synapse}})$ with $C = 1.0\text{nF}, R = 0.3\text{G}\Omega, V_{\text{leak}} = -60\text{mV}$
Voltage-gated channels	$g_{\text{channel}}(t,V) = \bar{g}m^P h$ $\frac{dm}{dt} = \alpha(1-m) - \beta m, \quad \tau = \frac{1}{\alpha+\beta}, \quad m_\infty = \frac{\alpha}{\tau}$ Exponential(Exp): $\alpha(V) = Ae^{B(V_m - V_0)} + C$ Sigmoid(Sig): $\alpha(V) = \frac{A}{1+e^{B(V_m - V_0)}}$ Linoid(Lin): $\alpha(V) = \frac{A(V_m - V_0)}{e^{B(V_m - V_0)} - 1}$
AMPA	$g_{\text{synapse}}(t,V) = we^{-\frac{t}{\tau_1}}$ with $t_1 = 30\text{ms}, w = 1, V_{\text{synapse}} = 5\text{mV}$
GABA	$g_{\text{synapse}}(t,V) = we^{-\frac{t}{\tau_1}}$ with $t_1 = 100\text{ms}, w = 2, V_{\text{synapse}} = 5\text{mV}$
Parallel fiber input	Model PC connected with all grcs.
Stellate cell input	Model PC connected with a SC.

Neuron Model	
Name	Stellate cell (SC)
Type	Hodgkin-Huxley
Dynamics	$I_{\text{applied}} = C\frac{dV}{dt} + \frac{1}{R}(V - V_{\text{leak}}) + \sum_{\text{channel}} g_{\text{channel}}(V - V_{\text{channel}}) + \sum_{\text{synapse}} g_{\text{synapse}}(V - V_{\text{synapse}})$ with $C = 1.0\text{nF}, R = 0.3\text{G}\Omega, V_{\text{leak}} = -60\text{mV}$

Voltage-gated channels	$g_{\text{channel}}(t,V) = \bar{g} m^P h$ $\frac{dm}{dt} = \alpha(1-m) - \beta m, \quad \tau = \frac{1}{\alpha+\beta}, \quad m_\infty = \frac{\alpha}{\tau}$ Exponential(Exp): $\alpha(V) = Ae^{B(V_m - V_0)} + C$ Sigmoid(Sig): $\alpha(V) = \frac{A}{1+e^{B(V_m - V_0)}}$ Linoid(Lin): $\alpha(V) = \frac{A(V_m - V_0)}{e^{B(V_m - V_0)} - 1}$
AMPA	$g_{\text{synapse}}(t,V) = we^{-\frac{t}{\tau_1}}$ with $t_1 = 30\text{ms}, w = 1, V_{\text{synapse}} = 5\text{mV}$
Parallel fiber input	Model PC connected with all grcs.

Parameter values of voltage-gated channels for model PC and SC											
Channel	V_{channel} (mV)	P				A (ms^{-1})	B (ms^{-1})	C (ms^{-1})	V_0 (mV)	Constraints	$\bar{g}$ (nS)
Na^+	55	3	m	α	Lin	1.0	-0.1		35		120
				β	Exp	4.0	-1/18		60		
			h	α	Exp	0.07	-0.05		60		
				β	Sig	1.0	-0.1		30		
K^+	-72	3	m	α	Lin	-0.01	-0.01		50		36
				β	Exp	0.125	-0.0125		60		
			h	α	Lin	-0.01	-0.01		50		
				β	Exp	0.125	-0.0125		60		

Bibliography

Albus J. S. A theory of cerebellar function. Math Biosci, 10:25–61, 1971.

Attwell P. J. E., Rahman S., and Yeo C. H. Acquisition of eyeblink conditioning is critically dependent on normal function in cerebellar cortical lobule hvi. J. Neurosci., 21:5715–5722, 2001.

Baker S., Olivier E., and Lemon R. Coherent oscillations in monkey motor cortex and hand muscle emg show task-dependent modulation. J. Physiol., 501:225–241, 1997.

Bower J. M. and Beeman D. The book of GENESIS: Exploring Realistic Neural Models with the GEneral NEural SImulation System. TELOS, New York, 1995.

Brickley S. G., Cull-Candy S. G., and Farrant M. Single-channel properties of synaptic and extrasynaptic $GABA_A$ receptors suggest differential targeting of receptor subtypes. J Neurosci, 19:2960–2973, 1999.

Brickley S. G., Misra C., Mok M. H., Mishina M., and Cull-Candy S. G. NR2B and NR2D subunits coassemble in cerebellar golgi cells to form a distinct NMDA receptor subtype restricted to extrasynaptic sites. J. Neurosci., 23:4958–4966, 2003.

Buonomano D. V. and Mauk M. D. Neural network model of the cerebellum: Temporal discrimination and the timing of motor responses. Neural Comput, 6:38–55, 1994.

Christian K. M. and Thompson R. F. Neural substrates of eyeblink conditioning: Acquisition and retention. Learn Mem, 11:427–455, 2003.

Courtemanche R., Pellerin J.-P., and Lamarre Y. Local field potential oscillations

in primate cerebellar cortex: modulation during active and passive expectancy. J. Neurophysiol., 88:771–782, 2002.

Courtemanche R., Chabaud P., and Lamarre Y. Synchronization in primate cerebellar granule cell layer local field potentials: basic anisotropy and dynamic changes during active expectancy. Front Cell Neurosci, 3:1–9, 2009.

Csicsvari J., Henze D., Jamieson B., Harris K., Sirota A., Barthó P., Wise K., and Buzsáki G. Massively parallel recording of unit and local field potentials with silicon-based electrodes. J Neurophysiol., 90(2):1314–1323, 2003.

Cull-Candy S. G., Brickley S. G., Misra C., Feldmeyer D., Momiyama A., and Farrant M. NMDA receptor diversity in the cerebellum: identification of subunits contributing to functional receptors. Neuropharmacology, 37:1369–1380, 1998.

D'Angelo E. The critical role of golgi cells in regulating spatio-temporal integration and plasticity at the cerebellum input stage. Frontiers in Neurosci., 2:35–46, 2008.

Daniel M., Wolpert R., Miall C., and Kawato M. Internal models in the cerebellum. Trends in Cognitive Sciences, 2:338–347, 1998.

Dieudonné S. Submillisecond kinetics and low efficacy of parallel fibre-golgi cell synaptic currents in the rat cerebellum. J. Physiol., 510:845–866, 1998.

Donoghue J., Sanes J., Hatsopoulos N., and G G. G. Neural discharge and local field potential oscillations in primate motor cortex during volun- tary movement. J. Neurophysiol., 79:159–173, 1998.

Dugué G. P., Brunel N., Hakim V., Schwartz E., Chat M., Lévesque M., Courtemanche R., Léna C., and Dieudonné S. Electrical coupling mediates tunable low-frequency oscillations and resounance in the cerebellar golgi cell network. Neuron, 61:126–139, 2009.

Ekerot C. and Kanoa M. Long-term depression of parallel fibre synapses following stimulation of climbing fibres. Brain Res, 342:357–360, 1985.

Freeman J. H. J. and Muckler A. S. Developmental changes in eyeblink conditioning and neuronal activity in the pontine nuclei. Learn Mem, 10:337–345, 2003.

Geurts F. J., De Schutter E., and Dieudounné S. Unraveling the cerebellar cortex: cytology and cellular physiology of large-sized interneurons in the granular layer. Cerebellum, 2: 290–299, 2003.

Hartmann M. J. and Bower J. M. Oscillatory activity in the cerebellar hemispheres of unrestrained rats. J Neurophysiol, 80:1598–1604, 1998.

Hesslow G. and Ivarsson M. Suppression of cerebellar purkinje cells during conditioned responsesin ferrets. NeuroReport, 5:649–652, 1994.

Hesslow G. and Yeo C. H. The functional anatomy of skeletal conditioning. In:A Neuroscientist's Guide to Classical Conditioning. Springer-Verlag, New York, 2002.

Hirano T. Effects of postsynaptic depolarization in the induction of synaptic depression between a granule cell and a purkinje cell in rat cerebellar culture. Neurosci. Lett., 119: 145–147, 1990.

Ito M. Long-term depression. Annu Rev Neurosci, 12:85–102, 1989.

Ito M. Control of mental activities by internal models in the cerebellum. Nat Rev Neurosci., 9:304–313, 2008.

Ito M. and Kano M. Long-lasting depression of parallel fiber-purkinje cell transmission induced by conjunctive stimulation of parallel fibers and climbing fibers in the cerebellar cortex. Neuroscience Letters, 33:253–258, 1982.

Ito M. The Cerebellum and Neuronal Control. Raven Press, New York, 1984.

Ivry R. B. The representation of temporal information in perception and motor control. Curr Opin Neurobiol, 6:851–857, 1996.

Jirenhed D.-A. and Hesslow G. Learning stimulus intervals 窶尿 daptive timing of conditioned purkinje cell responses. Cerebellum., DOI:10.:1007/s12311–011–0264–3, 2011.

Jirenhed D.-A., Bengtsson F., and Hesslow G. Acquisition, extinction, and reacquisition of a cerebellar cortical memory trace. J. Neurosci., vol.27:pp.2493–2502, 2007.

Jörntell H. and Ekerot C.-F. Reciprocal bidirectional plasticity of parallel fiber receptive fields in cerebellar purkinje cells and their afferent interneurons. Neuron, 34:797–806, 2002.

Kadotani H., Hirano T., Masugi M., Nakamura K., Nakao K., Katsuki M., and Nakanish S. Motor discoordination results from combined gene disruption of the NMDA receptor NR2A and NR2C subunits. J. Neurosci., 16:7859–7867, 1996.

Kalmbach B., Davis T., Ohyama T., Riusech F., Nores W., and Mauk M. Cerebellar cortex contributions to the expression and timing of conditioned eyelid responses. J. Neurophysiol., 103:2039–2049, 2010.

Kondo S. and Marty A. Synaptic currents at individual connections among stellate cells in rat cerebellar slices. J Physiol (Lond), 509.1:221–232, 1998.

Kotani S., Kawahara S., and Kirino Y. Purkinje cell activity during learning a new timing in classical eyeblink conditioning. Brain Res., 994:193–202, 2003.

Lange W. Regional differences in the distribution of Golgi cells in the cerebellar cortex of man and some other mammals. Cell Tissue Res, 153:219–226, 1974.

Linden D. and Connor J. Participation of postsynaptic pkc in cerebellar long-term depression in culture. Science, 254:1656–1659, 1991.

Llano I., Marty A., Armstrong C. M., and Konnerth A. Synaptic- and agonist-induced excitatory currents of Purkinje cells in rat cerebellar slices. J Physiol (Lond), 434:183–213, 1991.

Maass W., Natschläger T., and Markram H. Real-time computing without stable states: a new framework for neural computation based on perturbations. Neural Comput, 14: 2531–60, 2002.

MacKay W. and Mendonca A. Field potential oscillatory bursts in parietal cortex before and during reach. Brain Res., 18;704(2):167–174, 1995.

Maex R. and De Schutter E. Synchronization of Golgi and granule cell firing in a detailed network model of the cerebellar granule cell layer. J Neurophysiol, 80:2521–2537, 1998.

Marr D. A theory of cerebellar cortex. J Physiol (Lond), 202:437–470, 1969.

Mauk M. D. and Donegan N. H. A model of Pavlovian eyelid conditioning based on the synaptic organization of the cerebellum. Learn Mem, 3:130–158, 1997.

McCormick D. A. and Thompson R. F. Cerebellum: Essential involvement in the classically conditioned eyelid response. Science, 223:296–299, 1984.

Medina J. F. and Mauk M. D. Computer simulation of cerebellar information processing. Nat Neurosci, 3:1205–1211, 2000.

Medina J. F., Garcia K. S., Nores W. L., Taylor N. M., and Mauk M. D. Timing mechanisms in the cerebellum: Testing predictions of a large-scale computer simulation. J Neurosci, 20:5516–5525, 2000.

Mehring C., Rickert J., Vaadia E., Oliveira S. C.d, Aertsen A., and Rotter S. Inference of hand movements from local field potentials in monkey motor cortex. Nat Neurosci., 6(12):1253–1254, 2003.

Misra C., Brickley S. G., Farrant M., and Cull-Candy S. G. Identification of subunits contributing to synaptic and extrasynaptic NMDA receptors in golgi cells of the rat cerebellum. J. Physiol., 1:147–162, 2000.

Mugnaini E. The length of cerebellar parallel fibers in chicken and rhesus monkey. J. Comp. Neurol., 220:7–15, 1983.

Mugnaini E., Atluri R. L., and Houk J. C. Fine structure of granular layer in turtle cerebellum with emphasis on large glomeruli. J Neurophysiol, 37:1–29, 1974.

Murthy V. and Fetz E. Oscillatory activity in sensorimotor cortex of awake monkeys: synchronization of local field potentials and relation to behavior. J Neurophysiol., 76(6): 3949–3967, 1996.

O'Connor S., Berg R., and Kleinfeld D. Coherent electrical activity between vibrissa sensory areas of cerebellum and neocortex is enhanced during free whisking. J. Neurophysiol., 87:2137–2148, 2002.

Oscarsson O. Spatial distribution of mossy and climbing fibre inputs into the cerebellar cortex. In Creutzfeldt O., editor, Afferent and intrinsic organization of laminated structures in the brain, pages 34–42. Springer-Verlag, 1976.

Palay S. L. and Chan-Palay V. Cerebellar cortex: cytology and organization. Springer-Verlag, New York and Heidelberg and Berlin, 1974.

Palkovits M., Magyar P., and Szentágothai J. Quantitative histological analysis of the cerebellar cortex in the cat II cell numbers and densities in the granular layer. Brain Res, 32:13–32, 1971.

Pellerin J.-P. and Lamarre Y. Local field potential oscillations in primate cerebellar cortex during voluntary movement. J Neurophysiol, 78:3502–3507, 1997.

Pesaran B., Pezaris J., Sahani M., Mitra P., and Andersen R. Temporal structure in neuronal activity during working memory in macaque parietal cortex. Nat Neurosci, 5: 805–811, 2002.

Pichitpornchai C., Rawson J., and Rees S. Morphology of parallel fibres in the cerebellar cortex of the rat: an experimental light and electron microscopic study with biocytin. J. Comp. Neurol., 342:206–220, 1994.

Rancillac A. and Cr??pel F. Synapses between parallel fibres and stellate cells express long-term changes in synaptic efficacy in rat cerebellum. J. Physiol., 554:707–720, 2004.

Rougeul A., Bouyer J., Dedet L., and Debray O. Fast somato-parietal rhythms during combined focal attention and immobility in baboon and squirrel monkey. Electroencephalogr Clin Neurophysiol., 46(3):310–319, 1979.

Silver R. A., Traynelis S. F., and Cull-Candy S. G. Rapid-time-course miniature and evoked excitatory currents at cerebellar synapses *in situ*. Nature, 355:163–166, 1992.

Stuart G. J. and Sakmann B. Active propagation of somatic action potentials into neocortical pyramidal cell dendrites. Nature, 367:69–72, 1994.

Svensson P., Ivarsson M., and Hesslow G. Involvement of the cerebellum in a new temporal property of the conditioned eyeblink response. Prog Brain Res., 124:317–323, 2000.

Svensson P., Jirenhed D.-A., Bengtsson F., and Hesslow G. Effect of conditioned stimulus parameters on timing of conditioned purkinje cell responses. J. Neurophysiol., 103:1329–1336, 2010.

Thompson R. The neurobiology of learning and memory. Science, 233:941–947, 1986.

Wong R. K. S. and Stewart M. Different firing patterns generated in dendrites and somata of ca1 pyramidal neurones in guinea-pig hippocampus. J. Physiol., 457:675–687, 1992.

Yamazaki T. and Tanaka S. A spiking network model for passage-of-time representation in the cerebellum. Eur. J. Neurosci., 26:2279–2292, 2007a.

Yamazaki T. and Tanaka S. Computational models of timing mechanisms in the cerebellar granular layer. Cerebellum, 8:423–432, 2009.

Yamazaki T. and Tanaka S. Neural modeling of an internal clock. Neural Comput, 17: 1032–1058, 2005.

Yamazaki T. and Tanaka S. The cerebellum as a liquid state machine. Neural Netw, 20: 290–297, 2007b.

List of Publications Related to the Disertation

1. 本多武尊, 山崎匡, 田中繁, 西野哲朗 ”小脳スパイキングネットワークモデルにおける条件刺激強度依存性タイミング制御”, 情報処理学会論文誌：数理モデル化と応用 (TOM), Vol.3, No.2, pp.1-10, 2010

2. 本多武尊, 山崎匡, 田中繁, 西野哲朗 ”小脳顆粒層をモデル化したスパイキングネットワークの研究：NMDA 受容体を介した同期発火状態と時間表現状態の遷移”, 電子情報通信学会論文誌 D, Vol.J91-D, No.11, pp.2709-2718, 2008

3. Takeru Honda, Tadashi Yamazaki, Shigeru Tanaka, Soichi Nagao and Tetsuro Nishino. ”Phase diagram of cerebellar granular layer dynamics: a model study”, no. p1-q24, The Joint Conference of: The 33rd annual Meeting of the Japan Neuroscience Society, The 53rd Annual Meeting of Japanese Society for Neurochemistry, The 20th Annual Meeting of Japanese Neural Network Society (Neuro2010), Kobe, Japan, September 2-4, 2010.

4. Takeru Honda, Tadashi Yamazaki, Shigeru Tanaka, Soichi Nagao and Tetsuro Nishino. ”A spiking network model of the cerebellar granular layer shows stimulus-dependent state transition between synchronized oscillation and randomly repetitive burst”, 7th Forum of European Neuroscience Program No. 052.17. Amsterdam, The Neitherlands, July 3-7, 2010.

5. Takeru Honda, Tadashi Yamazaki, Shigeru Tanaka and Tetsuro Nishino ”A Possible mechanism for controlling timing representation in the cerebellar cortex”, 2010 June

6-9, Seventh International Symposium on Neural Networks (ISNN 2010), Shanghai, China, 2010.

6. Takeru Honda, Tadashi Yamazaki, Shigeru Tanaka and Tetsuro Nishino "Strength of a conditional stimulus controls the timing of a conditional response: Computational study of the dynamics of a cerebellar spiking network model", 2009 October 17-21, Society for Neuroscience (SfN 2009), Program no. 367.3/DD25, Neuroscience Meeting Planner, Chicago, USA, 2009

7. Takeru Honda, Tadashi Yamazaki, Shigeru Tanaka and Tetsuro Nishino "The dynamics of a spiking network model for the cerebellar granular layer: stimulus-strength-dependent transition of states between synchronized oscillation and random repetitive activation", 2008 November 15-19, Society for Neuroscience (SfN 2008), Program no. 777.17/PP12, Neuroscience Meeting Planner, Washington, DC, USA, 2008

8. 松野香菜子, 本多武尊, 眞鍋秀聡, 田中繁, 西野哲朗 "FPGA 上に実装した小脳ネットワークモデルにおけるタイミングメカニズムの研究", 電子情報通信学会ニューロコンピューティング研究会, 信学技報, vol. 109, no. 363, NC2009-72, pp. 7-12, 2010

9. 本多武尊, 山崎匡, 田中繁, 西野哲朗 "小脳スパイキングネットワークモデルにおける条件刺激強度依存性タイミング制御", 情報処理学会数理モデル化と問題解決研究会 (MPS75), MPS75-30, 2009

10. 本多武尊, 山崎匡, 田中繁, 西野哲朗 "小脳顆粒層のスパイキングネットワークモデルの研究：条件刺激強度依存性タイミング制御", 日本神経回路学会第 19 回全国大会 (JNNS2009), 日本神経回路学会第 19 回全国大会講演論文集, O2-3, pp. 64-65, 2009

11. 本多武尊, 山崎匡, 田中繁, 西野哲朗 "小脳顆粒層のスパイキングネットワークモデルにおける状態遷移とタイミングメカニズムに関する研究", 電子情報通信学会ニューロコンピューティング研究会, 信学技報, vol. 107, no. 413, NC2007-95, pp. 49-54, 2008